Modeling and Analysis of the Impact of Wind Power Integration into the Grid on Power Quality (Case Study: Adama I wind farm)

Metasebia Fisseha Yemataw

A Thesis Submitted to the Department of Electrical Power and Control Engineering School of Electrical Engineering and Computing

Presented in Partial Fulfillment of the Requirement for the Degree of Master's of Science in Electrical Power and Control Engineering

(Power System Engineering)

Office of Graduate Studies

Adama Science and Technology University

July, 2024

Adama, Ethiopia

Modeling and Analysis of the Impact of Wind Power Integration into the Grid on Power Quality (Case Study: Adama I wind farm)

Metasebia Fisseha Yemataw

Advisor: Dr.Prathibha E.

A Thesis Submitted to the Department of Electrical Power and Control Engineering School of Electrical Engineering and Computing

Presented in Partial Fulfillment of the Requirement for the Degree of Master's of Science in Electrical Power and Control Engineering

(Power System Engineering)

Office of Graduate Studies

Adama Science and Technology University

July, 2024

Adama, Ethiopia

APPROVAL PAGE

Thesis I, the advisor of the thesis entitled "Modeling and Analysis of the Impact of Wind Power Integration into the Grid on Power Quality" and developed by Metasebia Fisseha, hereby certify that the recommendation and suggestions made by the board of examiners are appropriately incorporated into the final version of the thesis.

Dr.Prathibha E	____________	05/20/2024
Major Advisor	Signature	Date

We, the undersigned, members of the Board of Examiners of the thesis by Metasebia Fisseha have read and evaluated the thesis entitled "Modeling and Analysis of the Impact of Wind Power Integration into the Grid on Power Quality" and examined the candidate during open defense. This is, therefore, to certify that the thesis is accepted for partial fulfillment of the requirement of the degree of Master of Science in Electrical Power and Control Engineering.

Dr. Negasa Muleta	____________	06/20/2024
Chairperson	Signature	Date
Prof. Ravikumar Hiremath		06/3/2024
Internal Examiner	Signature	Date
____________________	____________________	____________________
External Examiner	Signature	Date

Final approval and acceptance of the thesis is contingent upon submission of its final copy to the Office of Postgraduate Studies (OPGS) through the Department Graduate Council (DGC) and School Graduate Committee (SGC).

____________________	____________________	____________________
Department Head	Signature	Date
____________________	____________________	____________________
School Dean	Signature	Date
____________________	____________________	____________________
Office of Postgraduate Studies, Dean	Signature	Date

DECLARATION

I hereby declare that this Master Thesis entitled "Modeling and Analysis of the Impact of Wind Power Integration into the Grid on Power Quality" is my original work. That is, it has not been submitted for the award of any academic degree, diploma or certificate in any other university. All sources of materials that are used for this thesis have been duly acknowledged through citation.

____________________	____________________	____________
Name of the student	Signature	Date

RECOMMENDATION

I, the advisor of this thesis, hereby certify that I have read the revised version of the thesis entitled “Modeling and Analysis of the Impact of Wind Power Integration into the Grid on Power Quality” prepared under my guidance by Metasebia Fisseha submitted in partial fulfillment of the requirements for the degree of Mater’s of Science in Electrical Power and Control Engineering. Therefore, I recommend the submission of revised version of the thesis to the department following the applicable procedures.

Dr.Prathibha E	___________	5/20/2024
Advisor	Signature	Date

ACKNOWLEDGEMENTS

First and foremost, I would like to give all glory and honor to my Almighty God, who has given me the courage, patience, potential, and wisdom to complete my master's thesis. I would like to acknowledge the invaluable support and guidance of my research advisor, Dr.Prathibha.E, whose expertise and encouragement have been instrumental in shaping this research. Their mentorship and insights have been invaluable throughout this journey.

I am also deeply grateful to my family for their unwavering support, understanding, and patience. Their love and encouragement have been a constant source of strength and motivation, and I am truly fortunate to have them by my side.

TABLE OF CONTENTS

LIST OF TABLES

LIST OF FIGURES

LIST OF ACRONYMS

AC	Alternating Current
DC	Direct current
DFIG	Doubly Fed Induction Generator
DVR	Dynamic Voltage Restorer
FACTS	Flexible AC Transmission Systems
FFT	Fast Fourier Transformer
FRT	Fault Ride-Through
GSC	Grid Side Converter
HAWT	Horizontal axis wind turbines
IEC	International Electro-Electrotechnical Commissioning
IEEE	Institute of Electrical and Electronic Engineers
IGBT	Insulated Gate Bipolar Transistor
ITHD	current total harmonic distortion
MPPT	Maximum Power Point Tracking
MSC	Machine Side Converter
PCC	Point of common coupling
PI	Proportional-Integral
PMSG	Permanent magnet generator
PQ	Power Quality
PV	Photovoltaic

PWM	Pulse Width Modulation
RL	Resistance-Inductance
SCIG	Squirrel Cage Induction Generator
SMC	Sliding mode control
STATCOMs	Static Synchronous Compensator
SVCs	Static VAr Compensator
SVPWM	State Vector Pulse Width Modulation
THD	Total harmonic distortion
TSR	Tip speed ratio
VAWT	Vertical axis wind turbines
VSWT	Variable speed wind turbine
VTHD	Voltage total harmonic distortion
WECS	Wind Energy Conversion System
WRIG	Wound rotor induction generator

ABSTRACT

Wind energy is a key renewable resource worldwide that can lessen dependence on traditional diesel generators. Ethiopia, aspiring to be the power house of Africa has three wind farms under operation totaling 324 MW capacities, and two extra which are under commissioning and construction. Integrating wind farms into the grid presents challenges in system operation, control, stability, and power quality. This study focuses on Adama I wind powerplant, which uses a Permanent Magnet Synchronous Generator (PMSG) with a full-scale power converter for grid connection. Despite the benefits, the presence of power electronic converters and nonlinear loads causes harmonic distortion. In this study a sliding mode control scheme is proposed for the PMSG-based wind energy system. The Nonlinear Proportional-Integral form of Sliding Mode Control (SMC) offers robustness and disturbance rejection but it can increase harmonic distortion due to chattering. This study mitigates SMC drawbacks by selecting a suitable reaching law and incorporating an RL filter into the control design. Simulation results in MATLAB/Simulink confirm the effectiveness of the control strategy, improving stability, settling time from 0.06 to 0.0094, overshoot from 0.68% to 0.096%, and reducing total harmonic distortion from 8.23% to 4.43%. Stability analysis using Lyapunov theory shows enhanced dynamic performance metrics, meeting harmonic requirements for a stable system.

Keywords: *MATLAB-Simulink, Permanent Magnet Synchronous Generator, Sliding Mode Control, Total Harmonic Distortion*

CHAPTER ONE

1. INTRODUCTION

1.1 Background of the Study

The increasing population and industrialization in recent times have resulted in a notable increase in power demand, hence presenting a noteworthy obstacle to the production of electricity. (Maihemuti et al., 2021) Nonetheless, depending only on non-renewable energy sources, which account for most of the energy market, is constrained and may result in the atmospheric discharge of dangerous pollutants, such as carbon dioxide. These sources include natural gas, oil, coal, and nuclear power. The world's average temperature has increased due to this tendency, causing the greenhouse effect. Renewable energy sources, including wind, fuel cells, solar, biogas, biomass, tidal, and geothermal, have surfaced as possibilities to address this problem. These clean, plentiful energy sources compete with more established ones. Among them, wind energy production is the most reliable, and cost-effective. Wind turbines are modular and can be installed as single units or in large wind farms, making it easy to scale up or down depending on the electricity demand. (Laghari et al., 2020).

Wind power has been added fleetly worldwide due to reactionary energy reduction and environmental pollution. According to the Global Wind Energy Association, the total installed global capacity grew to 906 GW in 2022 with a time-on-time growth of 9%. The report also forecasts that 2023 should be the veritably first time to exceed 100 GW of new capacity added encyclopedically with a time- on- time growth of 15% (Abdelateef Mostafa et al., 2023) likewise, according to the Global Wind Energy Council, "Beyond the statistics, wind power is getting a completely capitalized, unsubsidized technology; successfully contending in the business against heavily subsidized reactionary and nuclear incumbents" (GWEC, 2018). Among the countries that are promoting wind as a renewable energy resource are 30 countries with further than 1 GW of installed capacity and nine countries with further than 10 GW, including China, USA, Germany, India, Spain.

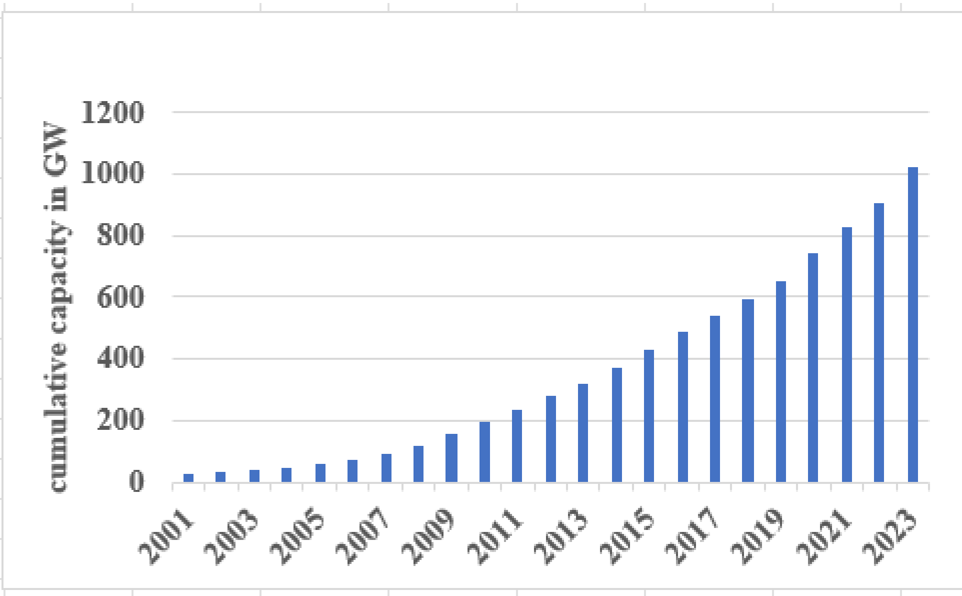

Figure 1. 1 Global wind power capacities (2001-2020)(Blaabjerg & Ma, 2017)

The renewable energy potential in Ethiopia includes hydro power, wind power, solar power, geothermal power, and biomass. however, countries, where power development is mostly focused on hydro can be severely affected by a drastic weather change in the case of dry hydrologic conditions. To ensure sustainable development and meet the growing electricity demand, Ethiopia is incorporating wind power plants alongside its existing hydroelectric facilities. By integrating wind power into its energy mix, Ethiopia aims to enhance its capacity to supply electricity while minimizing reliance on a single energy source. This diversified approach promotes sustainable development by leveraging the country's abundant wind resources and reducing the environmental impact associated with traditional power generation methods.

Consequently, large-scale wind farms are going to be integrated into the Ethiopian Electric Power Grid. Technically, wind energy could be the second most important resource next to hydro power for power generation. Ethiopia has great wind energy potential. According to the (Bekele & Abdela, 2012) study statistics, the capacity of 18,645 MW, 4,925 MW Power, and 2,005 MW with wind speed of 7.5~8 m/s,8~8.8 m/s, and more than 8.8 m/s respectively at a height of 50 m can be generated. This shows that there is a favorable condition to construct large-scale wind farms the shows that, from less than 300 MW of installed capacity 13 years ago, Ethiopia has now installed 4,284 MW of power generation capacity. Of this, 3,810 MW is from hydro installations, 324 MW is from wind, 7 MW is geothermal energy and there is also 143 MW of diesel power generation. However, the total renewable energy resource potential is Hydropower. 45,000 MW, wind~10,000 MW, solar~5,000 MW, geothermal potential ~ 5,000 to 10,000 MW, and others.(Hailu & Kumsa, 2020)

Adama-I wind farm is located approximately ninety-five km from Addis Ababa and seven km from Adama, at elevations of 1741~2173 m. The topographical position of the wind power project is 39° 12' 10" E, 8° 34' 18" N. The ground of the wind farm challenge particularly included shallow grass small shrubs and a few gravels. It is a positive site for wind power projects. The size of the Adama wind farm (phase-1) is 51MW, with 34 units, arranged in three groups and 1.5MW each unit. The rated generation capacity of the plant is 51MW (firm Energy of 157.4 GWh/year). Wind turbines utilize a permanent magnet generator, which is gearless and directly driven (Bekele & Abdela, 2012).

Figure 1. 2 Adama I Wind Farm

1.2 Statement of the Problem

The integration of wind power into the grid is crucial in meeting the power demand, but its intermittent nature and the presence of frequency converters pose challenges in maintaining the power quality of the grid. To address this issue, the ADAMA I wind farm has opted for a permanent magnet generator (PMSG), which can be direct-driven without a gearbox, resulting in reduced weight, mechanical losses, and maintenance requirements. Furthermore, PMSGs do not suffer from energy loss, unlike induction generators, which typically lose 20–30% of their energy. However, the generated power is routed through a full back-to-back converter to connect to the grid, which includes an alternating

Current(AC) to direct current(DC) vice versal frequency converter, and other nonlinear loads that inject harmonic distortion into the grid at the point of common coupling (PCC). This harmonic distortion adversely affects the waveform, purity, magnitude, and power factor of the voltage and current at PCC, leading to a degradation of the power quality of the grid. Voltage sags, in particular, harm the performance of power converters and electrical machines connected to the AC network.

To overcome the above problems develop and implement a sliding surface control mode, to optimize power quality and ensure grid stability when integrating PMSG wind turbines into the grid.

1.3 Objectives of the Thesis

1.3.1 General Objective

The main objective of this thesis is Modeling and Analysis of the Impact of Wind Power Integration into the Grid on Power Quality.

1.3.2 Specific Objectives

The specific objectives of this thesis are as follows:

- Mathematical modeling of a wind turbine.
- Develop a Sliding mode controller for the PMSG in the grid and machine side.
- Simulate the effectiveness of the model on power quality in the grid using MATLAB/SIMULINK
- Finally, depending on the result, conclude and offer suggestions.

1.4. Significant of the Study

Wind power is becoming increasingly cost-competitive with traditional fossil fuel sources of energy. However, the economic viability of wind power depends on its impact on power quality and grid stability. Investigating the impact of wind power integration on power quality can help identify cost-effective strategies to integrate wind power into the grid.

1.5 Scope and Limitation of the Study

This study aims to investigate and analyze the impact of wind power on harmonic distortion issues in the grid-connected Adama I wind farm. Specifically, the study examines the total harmonic distortion (THD) of voltages at common coupling (PCC) resulting from the AC/DC/AC frequency converter. The system model under study includes a PMSG-type wind turbine, machine side and grid side converter, RL filter, and a sliding mode control to improve THD value at PCC. In this study check the stability of the controller and harmonic distortion.

1.6 Thesis Organization

The whole part of this thesis is organized as follows:

- Chapter-one discussed general background, statement of the problem, objectives, methodologies, and thesis organizations.
- Chapter -two discussed about literature review.
- Chapter -three with modeling and analysis of system study.
- Chapter - four described about results analysis and discussions.
- Chapter - five presented all about the conclusion, recommendation, and future work.

CHAPTER TWO

2. LITERATURE REVIEW

2.1 Wind Turbine

Wind turbines are mechanical devices designed to harness the kinetic energy present in wind and convert it into usable electrical energy. These turbines achieve this conversion by utilizing specially designed blades that capture the force of the wind and translate it into rotational motion. This rotational motion is subsequently used to drive a generator, which generates electricity.

2.2 Classification of Wind Turbine

Based on the Orientation of their Blades:

- Horizontal axis wind turbines (HAWT) and
- Vertical axis wind turbines (VAWT)

2.2.1 Horizontal Axis Wind Turbines

Horizontal-axis wind turbines have blades that are positioned horizontally, perpendicular to the ground. HAWTs are the most widely used type of wind turbine due to their strength and efficiency. To accommodate the installation of the rotor shaft at the top and expose the turbine to stronger winds, the foundation of wind turbine towers must possess exceptional strength. This design requirement necessitates robust construction techniques capable of supporting the weight of the blades, gearbox, generator, and other components. Additionally, the assembly process involves the use of a substantial crane to hoist these components to the tower's uppermost section.

To mitigate potential issues caused by downward wind flow, horizontal-axis wind turbines are designed with an upwind configuration. This means that the rotor and blades face the oncoming wind. By doing so, the turbines can better withstand metal fatigue and reduce the risk of structural failure.

Furthermore, horizontal-axis wind turbines require additional yaw control mechanisms to track the wind direction accurately. Yaw control enables the turbine to align itself with the changing wind direction, ensuring optimal performance and preventing damage to the turbine components.

Figure 2. 1 Horizontal Axis Wind Turbines(Elkodama et al., 2023)

2.2.2 Vertical Axis Wind Turbines

Vertical Axis Wind Turbines (VAWT) are designed with blades arranged in a vertical helix-like configuration, which enables them to be less susceptible to frequent changes in wind direction compared to their horizontal axis counterparts. This is because the blades are rotated on a rotor shaft that is perpendicular to the ground. To address the challenge of mounting the shaft and its components on a tower, the shaft is typically mounted near ground level. While this makes maintenance easier and allows for installation in locations such as rooftops, it also leads to lower efficiency due to air drag and lower wind speeds at ground level compared to the higher wind speeds found at higher elevations

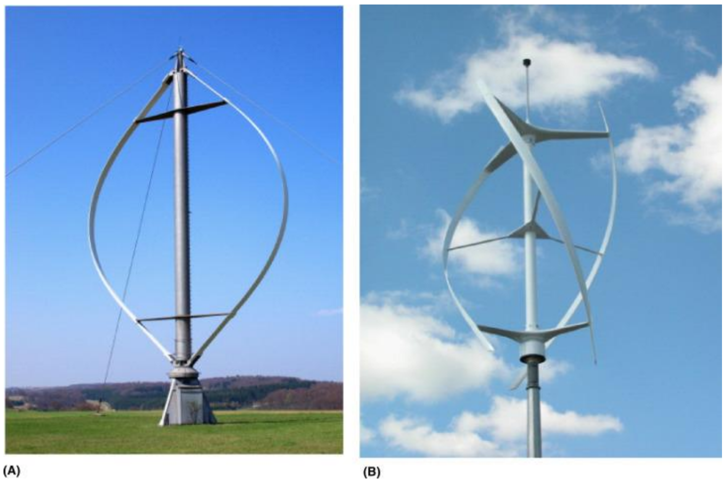

Figure 2. 2 Vertical axis wind turbines(M. Saad, 2014)

Speed Variation: According to the speed variation, wind turbines are classified as:

- Fixed Speed Wind Turbines (FSWT)
- Variable Speed Wind Turbines (VSWT)

Table 2. 1 Advantages and Disadvantages of FSWT and VSWT

Speed mode	Advantages	Disadvantages
Fixed speed	Simple, robust, reliable	Relatively low energy-conversion efficiency
	Low cost and maintenance	High mechanical stress
		High power fluctuations in the grid
Variable speed	High-energy conversion efficiency	Additional costs and losses due to the use of converters
	Improved power quality	More complex control system
	Reduced mechanical stress	

2.3 Wind Energy Conversion System Configurations

The wind energy system is comprised of two primary components: a wind turbine system and an electrical generator. The primary function of the wind turbine is to convert kinetic energy from the wind into mechanical energy, while the electrical generator transforms this mechanical energy into electrical energy that can be transmitted to the electrical grid. In recent years, various types of wind turbines have been developed, to improve their efficiency and performance. Wind turbines can operate at either fixed or variable speeds, depending on their design and application. (Senapati, 2014). Various types of generators used in wind turbines are listed and described in detail below.

2.3.1 Fixed Speed Wind Turbine

A Fixed Speed Wind Turbine (FSWT) is equipped with an induction generator either Squirrel Cage Induction Generator (SCIG) or Wound Rotor Induction Generator (WRIG) that is directly connected to the electrical grid. The rotor of an FSWT rotates at a constant speed determined by the frequency of the grid, the gear ratio, and the pole pairs of the generator. The induction generator absorbs reactive power from the grid, so a capacitor bank is necessary to provide reactive power compensation. A gearbox is used to transform the power from the turbine, which has a lower rotational speed, to the generator rotor, which has a higher rotational speed. A step-up unit transformer raises the generator's terminal voltage to a medium voltage level.

FSWT have several advantages, including their simplicity, robustness, and low cost of electrical components compared to other wind turbine types. However, they also have some disadvantages, such as uncontrollable reactive power consumption, mechanical stress, and limited power quality control. Additionally, because they operate at a fixed speed, any fluctuations in wind speed are transmitted as fluctuations in mechanical torque and electrical power on the grid. In weak electrical grids, these power fluctuations can lead to significant voltage fluctuations and line losses.(Rafiee et al., 2020).

Another disadvantage of FSWT is that they can experience loss of synchronism due to overspeed caused by voltage dips and an increase in reactive power consumption, especially after fault clearance. Generally, the dynamic stability of this type of generator cannot be improved, but preventive or corrective measures can be taken to limit acceleration during voltage dips by improving pitch control and providing reactive power support during and after the clearing of faults using Flexible AC Transmission Systems (FACTS) devices, such as Static VAr Compensator (SVCs) and Static Synchronous Compensator (STATCOMs). However, these measures can be costly.

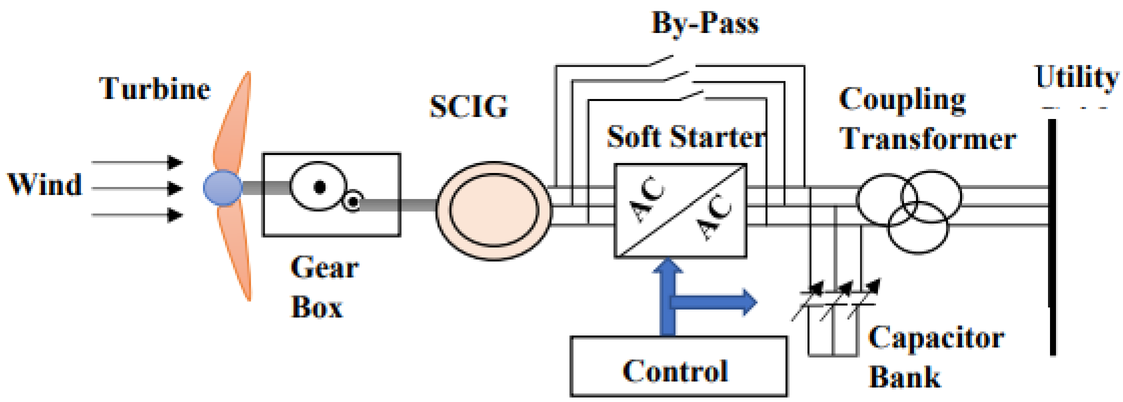

Figure 2. 3 Fixed speed wind turbine SCIG(Gustavo & Enrique, 2011)

2.3.2 Limited Variable Speed Turbine with Variable Rotor Resistance

A wind turbine with variable rotor resistance utilizes a wound rotor induction generator that is directly connected to the electrical grid. Similar to an FSWT, a capacitor provides reactive power compensation. One distinctive aspect of this configuration is its ability to incorporate a variable additional rotor resistance. This feature is achieved through an optically controlled converter that is installed on the rotor shaft. The converter allows for precise adjustment of the rotor resistance, offering flexibility in optimizing the turbine's performance and response to varying operating conditions. This results in a small variable speed range, typically ranging from 0-10% above synchronous speed.

These turbines can harvest more energy from a given wind environment than fixed-speed turbines because of their power and speed controls. This is because the variable rotor resistance allows the turbine to maintain a more optimal rotational speed for the given wind conditions, resulting in higher energy capture. Overall, wind turbines with variable rotor resistance can operate more efficiently than fixed-speed turbines and are becoming increasingly popular in the wind energy industry.

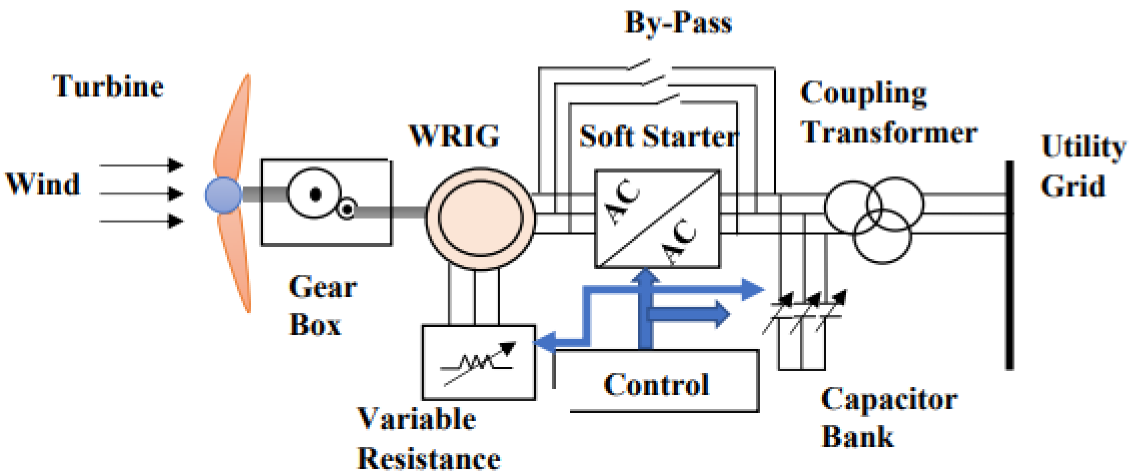

Figure 2. 4 Limited Variable Speed Turbines with Variable Rotor Resistance(Gustavo & Enrique, 2011)

2.3.3. Variable Speed Wind Turbine with Doubly-Fed Induction Generator

The Doubly Fed Induction Generator (DFIG) is connected to the grid through a power converter, which controls the flow of active and reactive power between the generator and the grid. The converter can adjust the rotor speed to match the wind speed, which allows the turbine to operate at its optimal efficiency.

One advantage of the DFIG is that it can provide reactive power support to the grid, which can help to stabilize the voltage and improve the overall stability of the grid. Additionally, because the power converter is located on the rotor side, only a small portion of the generated power needs to be converted, which reduces the size and cost of the power converter. However, the DFIG also has some disadvantages. The use of slip rings and brushes to connect the rotor windings to the power converter can lead to maintenance issues and reduced reliability. Additionally, the DFIG is not able to provide full power during grid faults, which can limit its effectiveness in certain situations. Despite these limitations, the DFIG remains a popular choice for variable-speed wind turbines due to its efficiency and flexibility. (Arachchige et al., 2017).

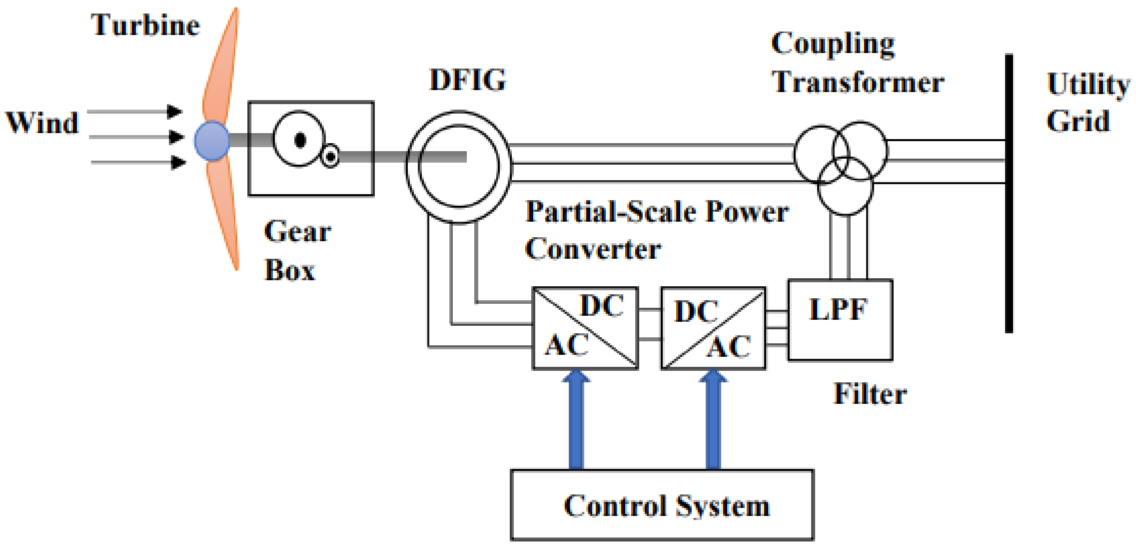

Figure 2. 5 Variable-Speed Wind Turbines with DFIG(Echiheb et al., 2022)

2.3.4 Variable Speed Wind Turbine with Full-Scale Power Converter

In this configuration, the wind turbine generator is connected to the electrical grid through a full-scale power converter, and the converter typically has the same power rating as the generator. One advantage of this type of wind turbine is that it can have a gearless configuration, which means it uses a low-speed synchronous generator with a large number of poles, eliminating the need for a gearbox.

This gearless configuration provides several benefits, including improved performance and reduced initial costs and maintenance requirements. Additionally, gearboxes can be a significant source of mechanical stress and failure in wind turbines, so eliminating them can increase the reliability and lifespan of the machine. However, this type of wind turbine also has some drawbacks, such as the need for a larger and heavier generator due to the low rotational speed, which can increase the cost of the turbine. Additionally, the power converter can be complex and expensive, which can also add to the overall cost of the system. Despite these limitations, the gearless configuration remains a popular choice for wind turbines due to its reliability and performance advantages. (Senapati, 2014).

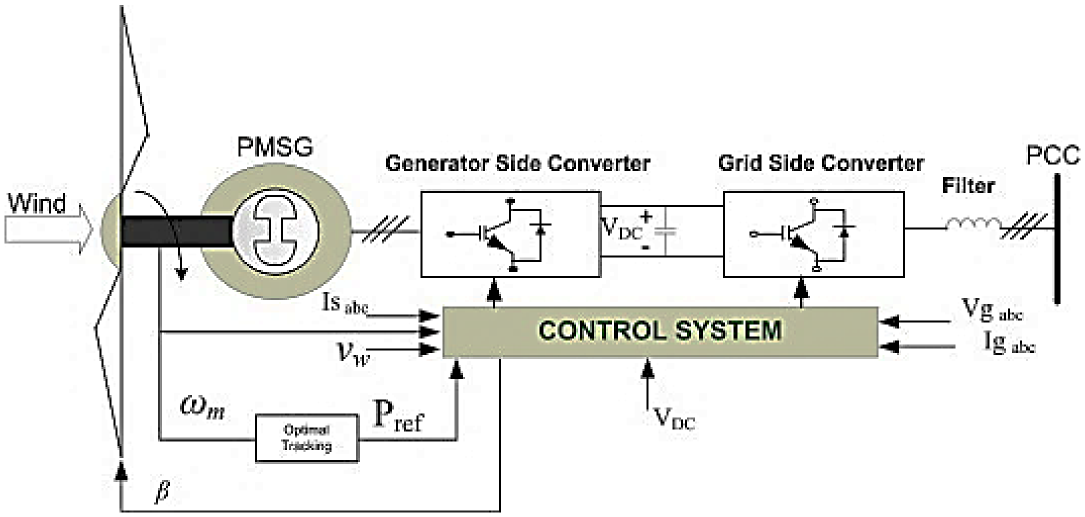

Figure 2. 6 Variable-Speed Wind Turbines with Full-Scale Power Converter(Kasem Alaboudy et al., 2013)

2.4 Main Parts of the Wind Generation System

Rotor and Hub: The rotor is a crucial component of a wind turbine, responsible for capturing the energy from the wind and converting it into mechanical energy. Typically, the rotor consists of three blades and a central hub that connects the blades to the rotor shaft. While other numbers of blades are possible, the three-blade configuration is the most common due to its optimal efficiency. The blades themselves are not solid, but rather hollow and made of lightweight yet strong composite materials. As wind turbines become larger and more powerful, there is a trend toward making the blades even bigger, lighter, and more robust. To optimize their aerodynamic performance, the blades are designed with a shape similar to an airfoil, like an airplane's wings. The blades can rotate around their axis up to 90 degrees, a movement known as pitch. This allows the turbine to adjust the angle of attack of the blades to optimize their performance and maintain a constant rotor speed in varying wind conditions. The pitch angle is controlled by the turbine's control system, which continuously monitors the wind speed and adjusts the pitch angle to maximize the energy output of the turbine. (Yıldız et al., 2015).The hub plays a crucial role in a wind turbine by connecting the blades to the rotor shaft and allowing them to rotate relative to the rest of the turbine body. It is a significant component of the turbine that is mounted on the rotor and is responsible for extracting energy from the wind. In addition to supporting the rotor blades, the hub is also responsible for controlling the pitch angle of the blades. By adjusting the pitch angle, the hub can optimize the performance of the turbine and maintain a constant rotor speed in varying wind conditions. (Hamzah et al., 2020).

Tower: Wind turbine towers are typically constructed from tubular steel, concrete, or steel lattice. Taller towers are advantageous because wind speeds are generally higher at greater heights, allowing turbines mounted on taller towers to capture more energy and generate more electricity. By elevating the turbine higher into the air, the turbine can access stronger and more consistent wind resources, improving its overall energy output and efficiency. This is particularly important in areas with low wind speeds or inconsistent wind patterns, as taller towers can help to increase the capacity factor of the turbine and make wind energy production more reliable and cost-effective. The choice of tower material depends on a variety of factors, including the turbine size, location, and cost considerations. Tubular steel towers are the most common type of tower used for wind turbines, while concrete and steel lattice towers are used in certain applications. Overall, wind turbine towers play a critical role in the performance and efficiency of wind turbines. By optimizing their design and construction, wind turbine manufacturers can maximize the energy output of their turbines and make wind energy an increasingly competitive source of renewable energy. (Ahmed et al., 2020).

Generator: The generator is a part that can convert the mechanical energy produced by the rotor rotation into electrical energy (Harish & Sant, 2021). It is comprised of a rotor and a stator.

Pitch System: When the wind speed exceeds the rated wind speed, the input power of the rotor can be limited to 1.5MW by adjusting the pitch angle of the blades. In that way, it can prevent the generator and converter system from overloading; when the wind speed is less than the rated wind speed, the blades' pitch angle is the smallest with the biggest capacity of absorbing wind power to increase the rotor's output and meet the requirements for power generating (Ahmed et al., 2020).

The pitch system is a critical component of a wind turbine that controls the angle of attack of the rotor blades. By adjusting the pitch angle of the blades, the turbine can optimize its performance in varying wind conditions and maintain a constant rotor speed. The pitch system typically consists of a set of hydraulic or electric actuators that are mounted on the hub of the rotor and connected to the blade root. These actuators are responsible for adjusting the pitch angle of each blade independently, allowing the turbine to respond to changes in wind speed and direction. The pitch system is controlled by a sophisticated control system that continuously monitors the wind speed and other environmental factors, as well as the performance of the turbine. Based on this information, the control system adjusts the pitch angle of the blades to optimize the turbine's energy output and protect it from damage. In addition to optimizing performance, the pitch system also plays a critical role in protecting the turbine from damage in high wind conditions. By adjusting the pitch angle, the turbine can reduce the aerodynamic forces acting on the blades and prevent excessive mechanical stress and damage.

Yaw System: The yaw system is a critical component of a wind turbine that allows it to rotate about its vertical axis and face the wind. By adjusting the yaw angle, the turbine can optimize its energy output and protect itself from damage in high wind conditions.The yaw system typically consists of a yaw drive, which is a motor or hydraulic system that rotates the nacelle, or the housing that contains the generator and other components, about its vertical axis. The yaw drive is controlled by a sophisticated control system that continuously monitors the wind direction and adjusts the yaw angle to ensure that the turbine is always facing the wind. In addition to optimizing the energy output of the turbine; the yaw system also plays a critical role in protecting the turbine from damage in high wind conditions. By facing into the wind, the turbine can reduce the aerodynamic loads acting on the blades and other components and prevent excessive mechanical stress and damage. When yawing is needed, two mutually independent sensors at the tail outside of the nacelle anemometer and wind vane detect the changes in wind speed and wind direction. The master control system calculates the bias of wind turbine generators and wind direction depending on the data collected by the anemometer and wind vane, then the yaw motor starts and the yaw system begins operating to make the wind turbine aligned to the wind. After the wind turbines are successfully aligned to the wind, the yaw braking system brakes.

2.5 Variable Speed Wind Turbine Operation Area

Based on the parameters given in this thesis work, the relationship between wind speed and power output is shown in Figure 2.8. There are three separate zones on the graph.

Parking Mode: The wind turbine will remain in parking mode due to inadequate electrical power provided by the PMSG system to offset the internal power losses in the system when the wind speed falls below the cut-in speed, which in this thesis case is 3 m/s. For this reason, a mechanical brake keeps the wind turbine in park mode.

Maximum Power Point Tracking (MPPT) Mode: The wind turbine system begins to operate and produce electricity when the wind speed exceeds the cut-in speed. The wind turbine's power capture efficiency is below its rated value due to the relatively low wind speed range in the MPPT mode. Therefore, to ensure maximum power capture efficiency, the MPPT control must be implemented. When the wind speed exceeds the case-study system's rated wind speed of 22 m/s, the MPPT mode comes to an end.

Constant Power Region: If the MPPT control is still used, the system's power output will exceed its rated power when the wind speed exceeds the rated value. This will further harm the power processing devices and PMSG by increasing their electrical stress. To maintain the system functioning within its rated output condition, the wind turbine blades' blade angle must be appropriately regulated in the strong wind range. This is a zone of constant power, as its name suggests.

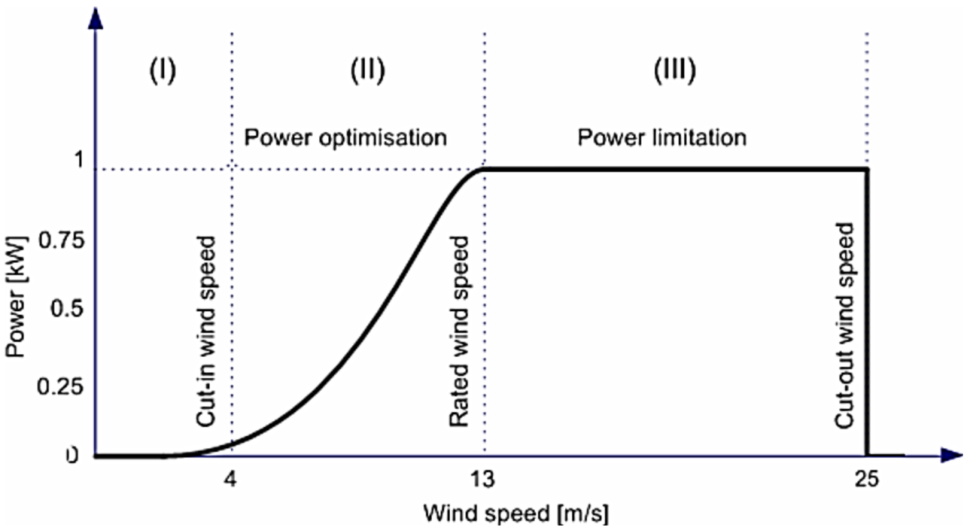

Figure 2. 7 Wind power output versus wind speed.(Rehman et al., 2018)

2.6 Power Quality

Institute of Electrical and Electronic Engineers (IEEE) Standard IEEE Std1100TM-2005 IEEE Recommended Practice for Powering and Grounding Electronic Equipment, defines power quality as (Blooming & Carnovale, 2006) “the concept of powering and grounding sensitive electronic equipment in a manner suitable for the operation of that equipment and compatible with the premise wiring system and other connected equipment.”

2.7 Power Quality Problem

2.7.1 Unbalanced Voltage:

Unbalanced Voltage: is a problem with power quality that occurs when the three phases of a power system that uses three phases have varying amounts, resulting in an uneven waveform. Unbalanced loads, faulty connections, or phase-to-ground faults can cause this asymmetry. Unbalanced current flow from uneven voltage levels in various system phases can cause equipment to overheat and operate less efficiently. Ground fault current flow can result from negative or zero-sequence components in the voltage waveform, damaging equipment and posing a safety risk.

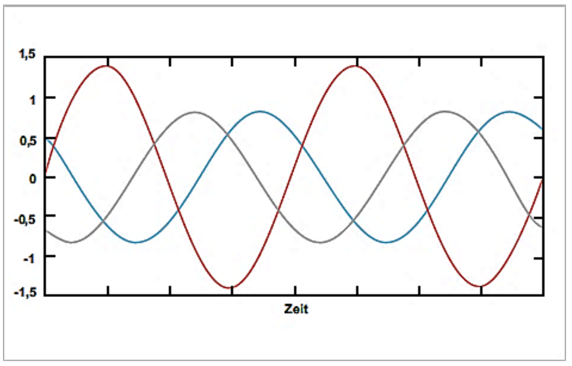

Figure 2. 8 Unbalanced Voltage(Grant et al., n.d.)

2.7.2 Voltage Sag:

Voltage Sag: an intermittent voltage drop that occurs for a few cycles to a few seconds below the standard level. An abrupt spike in load, a dip in grid voltage, or a system malfunction are the reasons behind it.

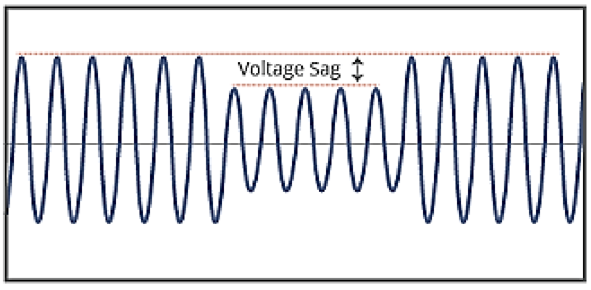

Figure 2. 9 Voltage Sag(Tang et al., 2022)

2.7.3 Voltage Swell:

A brief, few-cycle to few-second surge in voltage over the standard level is known as a voltage swell. It is brought on by abrupt shifts in load or the clearing of a system malfunction.

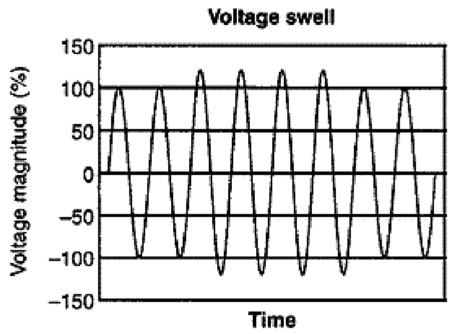

Figure 2. 10 Voltage Swell(Grant et al., n.d.)

2.7.4 Voltage Interruption:

Voltage interruption is a complete loss of voltage for a short time. It may take a few milliseconds to several minutes to occur and may be brought on by lightning strikes or distribution system faults. Equipment may reset or shut down as a result of this disruption, which could result in data loss or damage.

2.7.5 Harmonics:

Higher-frequency electrical impulses known as harmonics disrupt the power that utilities provide to residences and commercial buildings. Harmonics produced by electronic devices with nonlinear loads have the potential to harm electrical equipment and interfere with the operation of distribution equipment.

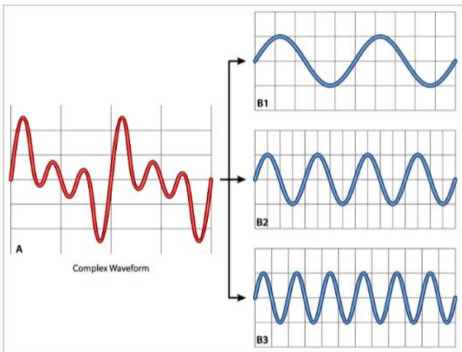

Figure 2. 11 Harmonic Signals(Singh et al., 1999)

The back-to-back converters of variable-speed wind turbines allow them to operate under varying wind speed conditions and allow for maximum power point tracking. However, the converters introduce harmonics into the grid. The level of harmonics can be reduced by filtering. One of the indices for measuring harmonics is the THD (Bekri et al., 2014).
The total harmonics distortion in bus voltage (VTHD) is defined as the ratio of the square root of the sum of squares of the rms value of the harmonic component, Vn to the rms value of the fundamental component V1(Dash et al., 2021)

$$v_{TH} = \sqrt{\frac{\sum_{n=odd} {v_n}^2}{{v_1}^2}}$$

Where h is the harmonic number, V1 is the fundamental harmonic and Vn is the n^{th} harmonic. The THD planning level for medium voltage is 6.5% and 3% for a high voltage system

The total harmonics distortion of line current (ITHD) is defined as the ratio of the square root of the sum of squares of the rms value of the harmonic component, Into the rms value of the fundamental component, I1(Dash et al., 2021)

2.8 Power Quality Standard

Institute of Electrical and Electronic Engineers (IEEE) Standard 519-1992, Recommended Practices and Requirements for Harmonic Control in Electrical Power Systems.

Table 2. 2 Voltage distortion limit

Bus voltage	Individual voltage distortion (%)	Total voltage distortion THD (%)
Below 69 KV	3.0	5.0
69KV to 161 KV	1.5	2.5
161 KV above	1.0	1.5

2.9 Sliding Mode Control

Besides, one of the suggested algorithms to control nonlinear systems such as wind turbines is the sliding mode control (SMC). The SMC has shown a promising result in achieving a high degree of reliability, accuracy, and stability, with a major flexibility during parameter variations. Pure SMC technique faces the chattering appearance. Therefore, several composite SMC architectures have been built in combination with other approaches, such as Fuzzy-sliding mode. Despite the ability to chatter reduction, these mixed methods necessitate complex application processes, especially at high power capacities systems such as the extended version of PMSG with several control loops. Within this framework, the main target of this paper, on the one hand, is to produce an appropriate design of variable speed wind turbine (VSWT) consisting of a five-phase PMSG instead of the conventional three-phase PMSG due to its various aforementioned advantages, and on the other hand, improve and enhance the effectiveness of proposed system, by involving an optimized sliding mode control that supervises the entire system of wind turbine and the connected grid supply, due to its high degree of robustness, ability of reducing the dynamic response time, and most of all its exploitation simplicity. Moreover, the proposed robust SMC algorithm consists of an enhancement method based on a new smooth switching function with an integral component to mitigate the chattering phenomenon and reduce the energy loss, thereby, improving the efficiency and accuracy in this work.

2.10 Related Works

(Dash et al., 2021) discussed the topic of power quality improvement in grid-connected wind systems with STATCOM. The authors delve into the various power quality issues, their sources, parameters, mitigation techniques, and standards. Through their investigation, they identify the high penetration of wind and the increasing use of nonlinear loads as sources of power quality distortion. To monitor the power quality, the authors employ various techniques, with a focus on monitoring harmonics. They use fast Fourier Transformer (FFT) analysis to calculate the THD at the PCC under two conditions: with STATCOM and without STATCOM. The authors conclude that the use of STATCOM results in a significant improvement in power quality. The paper may not thoroughly evaluate the performance of the STATCOM control scheme under dynamic conditions, such as rapid changes in wind speed

(Bubshait et al., 2017) discussed Power Quality Enhancement for a Grid Connected Wind Turbine Energy System. To enhance the power quality, the authors employ an algorithm that has been developed allowing a control structure that utilizes a four-leg inverter connected to the grid side, and the Proposed methodology of Conservative Power Theory decompositions. This option offers very flexible, powerful, and selectable functions for the inverter control by providing decoupled power and current references. exclude passive filters different tests are performed to validate the overall performance of the machine side and the grid side controllers during different wind speed conditions. From this paper the final result THD value of 2.68%.

(Molla & Kuo, 2020). Discussed enhancing voltage sag in grid-connected hybrid Photovoltaic (PV) -wind power systems using custom power devices. The authors investigate the intermittent nature of power generation, which is dependent on wind speed and leads to power fluctuations. Voltage sag is identified as a major power quality issue, and to mitigate this problem, a battery and SMES-based Dynamic Voltage Restorer (DVR) is used as a compensating device. The authors examine two scenarios of voltage sag: symmetrical and asymmetrical. They propose the use of the DVR to mitigate the voltage sag and enhance power quality in both scenarios. The paper lacks an in-depth discussion on the control strategies employed for effective voltage fluctuation compensation. A detailed analysis of control algorithms and their performance could enhance the understanding of the proposed method.

(Mohamed et al., 2019). Studied on Power Quality (PQ) analysis of wind turbines installed in the Hatay region of Turkey. Power quality parameters such as voltage, current, active, reactive, apparent power, and harmonics are measured, analyzed, and evaluated taking into consideration IEEE 519-1992 standards. A phenomenon linked to the distortion of the fundamental sine wave is known as harmonic disturbances. Power quality standards provide the upper bound on the distortion of the power supply's voltage and current waveforms that is permitted. Measurements and assessments of the power quality of a wind farm are made in this study. A wind farm has been installed with a total capacity of 36 MW and is constituted of 12 wind turbines. Every wind turbine generator has its own star-delta linked transformer, rated at 0.69/34.5 kV. Electrical parameters of wind farms such as voltage, current, frequency, active, reactive, apparent power, power factor, and harmonic distortions are given and analyzed.

CHAPTER THREE

3. METHODOLOGY AND SYSTEM DESCRIPTION

3.1 Methodology

The methodology flowchart for the research on Modeling and Analysis of the Impact of Wind Power Integration into the Grid on Power Quality outlines a structured approach to investigating the impact of wind power integration on power quality. It encompasses key steps such as research area identification, literature review, problem identification, data collection, simulation using Matlab Simulink, and result analysis. This flowchart provides a clear roadmap for conducting the study, ensuring a systematic and comprehensive research process from start to finish.

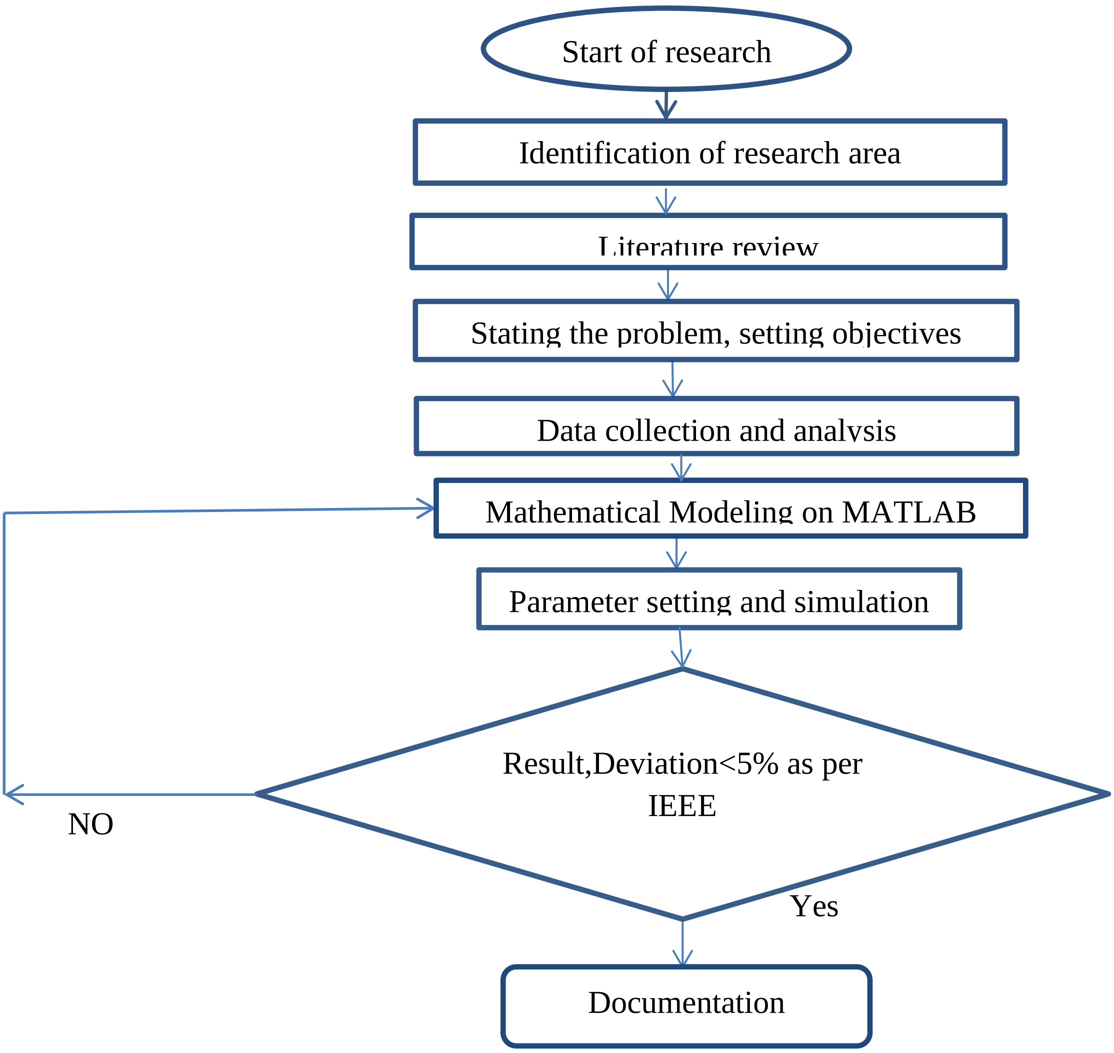

Figure 3. 1. Methodology of the proposed system

3.2 Analyzing Wind Speed Characteristics

Cut-in Wind Speed: Cut-in wind speed refers to the minimum wind speed at which a wind turbine starts generating electricity. The Cut-in speed of Adama-I wind power is 3 m/s. When the wind speed exceeds the cut-in speed, the wind turbine's blades start to rotate, and the generator begins producing electricity.

Rated Speed: Rated wind speed is the wind speed at which a wind turbine generates its maximum power output. The rated speed of the Adama-I wind power plant is 11 m/s. Wind turbines are designed to automatically adjust their blade pitch and rotor speed to maintain a constant power output as the wind speed varies around the rated wind speed.

Cut-out Speed: Cut-out speed refers to the wind speed at which a wind turbine stops generating electricity and shuts down for safety reasons. When the wind speed reaches the cutout speed, the wind turbine's control system triggers the blades to pitch out of the wind, and the turbine shuts down to prevent damage to the rotor and other components. The Cut-out wind speed of the Adama-I wind power plant is 22 m/s.

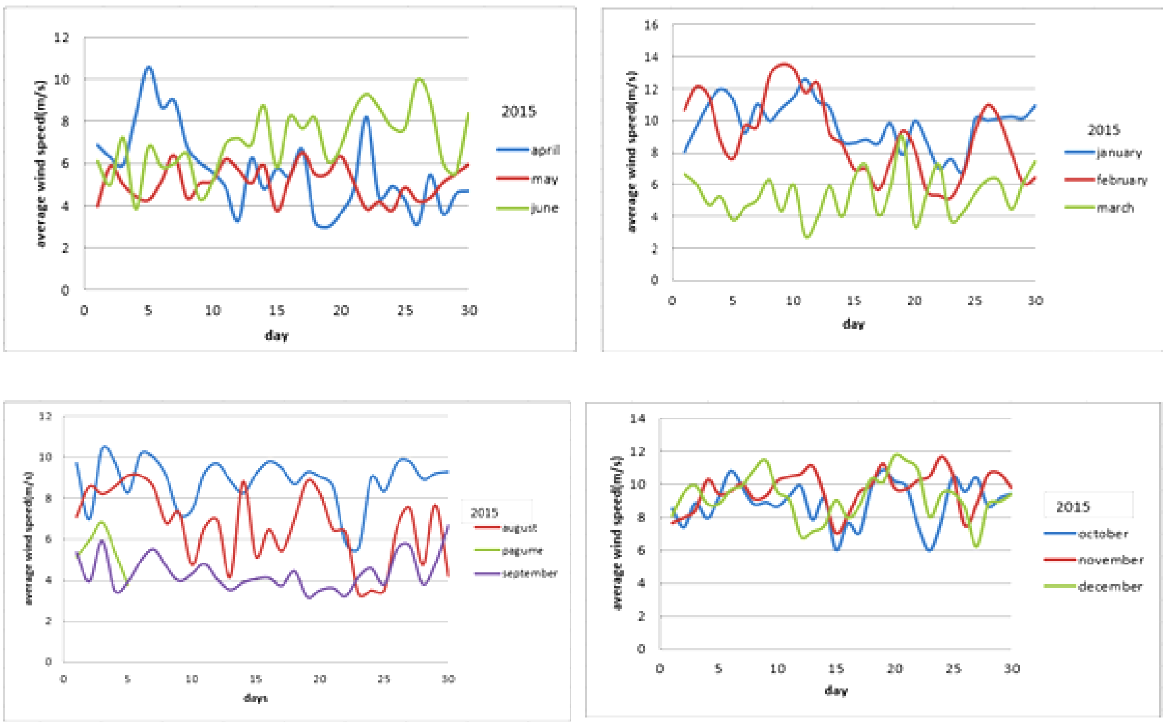

Figure 3. 2 Wind speed variation of Adama I wind farm 2015.

3.3 Existing Grid-connected Wind Farm

Adama I wind farm comprises three groups of 34 turbines, with a total installed capacity of 51MW. The wind farm also includes a 55MVA main power transformer, a 1600kVA unit transformer, and a 4.7Km 132KV single circuit overhead transmission line that feeds into the grid of the Nazret substation.

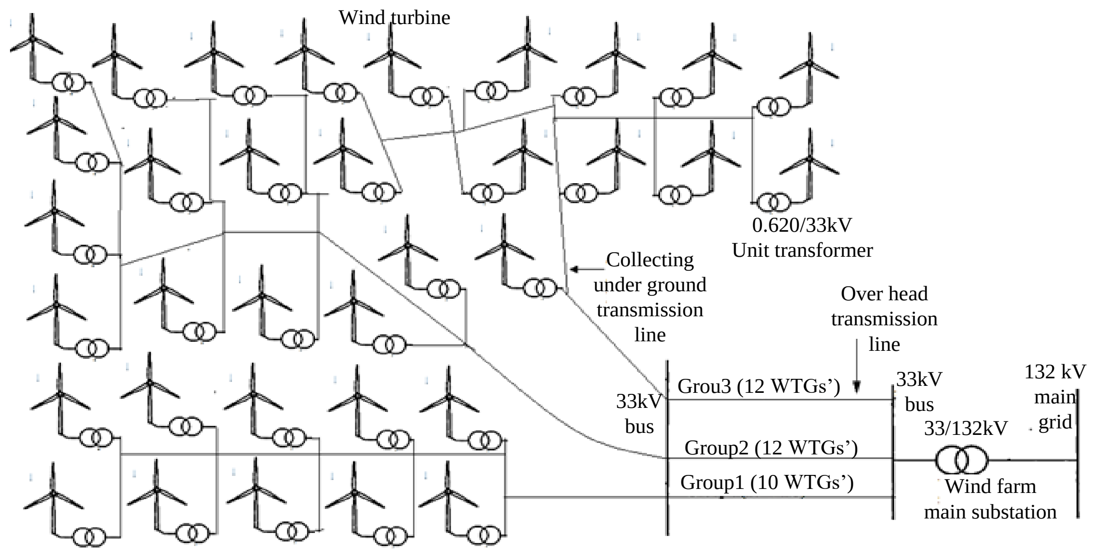

Figure 3. 3 Grid-connected Adama-I wind farm simple layout diagram

3.4. Wind Turbine Aerodynamic Modeling

The rotor of a wind turbine is a sophisticated aerodynamic device that absorbs and converts wind energy into mechanical energy. As demonstrated in Figure 3.4, Bernoulli's principle is used to easily understand the process. Aerodynamic power and torque are two characteristics of wind turbines. (Manyonge et al., 2012)

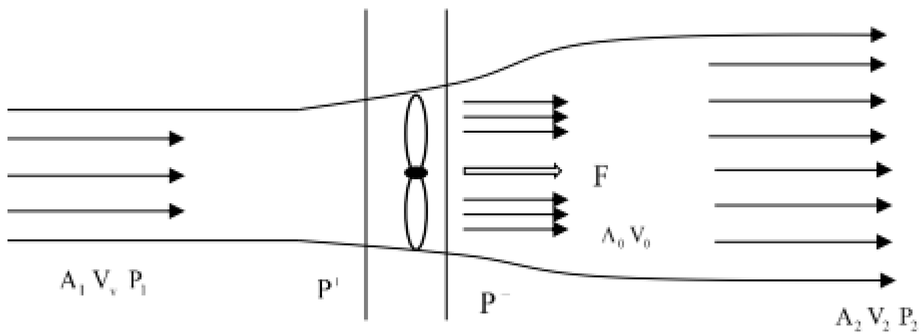

Figure 3. 4 Schematic of fluid flow through a disk-shaped actuator(Gharib-Yosry et al., 2021)

The wind crossing's aerodynamic power at a speed Vv, a wind disk radius R, and a surface A1 is given by:

$$P_w = \frac{1}{2}\rho\pi R^2 Vv^3 \tag{3.1}$$

Where ρ the air density in kilograms per cubic meter is, Vv is the wind speed in meters per second, and R is the blade radius in meters.

The mechanical power, Pm, generated by a wind turbine is determined by the power coefficient $C_{p.}$

$$Pm = Cp \times Pw = \frac{1}{2}\rho\pi R^2 Vv^3 Cp(\lambda,\beta) \tag{3.2}$$

where C_p is the power coefficient that indicates how efficiently the wind turbine captures energy from the wind and transforms it into mechanical energy. It is utilized to reduce the amount of power available at the wind turbines. Analytically, it can be represented as follows:

$$Cp(\lambda,\beta) = C_1 * (\frac{C_2}{\lambda_i} - C_3\beta - C_4\beta^{C_5} - C_6) * e^{\frac{-C_7}{\lambda_i}} \tag{3.3}$$

$$\lambda_i = \left[\frac{1}{\lambda + C_8\beta} - \frac{C_9}{\beta^3 + 1}\right]^{-1} \tag{3.4}$$

where λ is the tip speed ratio, β is the pitch angle, and C_1- C_9 are the wind turbine’s characteristic constants.

As shown in Equation (3.1), C_p depends on both pitch angle (β) and tip speed ratio (λ). The blade tip speed (i.e., the product of the angular speed of the rotor and the radius of the blade) to the incoming wind speed is known as the Tip speed ratio (TSR).(Zhang & Shu, 2010)(Manyonge et al., 2012) It can be mathematically expressed as follows:

$$\lambda = \frac{\Omega * R}{Vv} \tag{3.5}$$

Where Ω is the rotational angular speed of the rotor in *rad/sec* and R is the blade radius in meters.

The theoretical maximum power is given by:

$$P_{\max} = \frac{1}{2}\rho\pi R^2 Vv^3 Cp_{\max}(\lambda,\beta) = 0.3644\pi R^2 Vv^3 \quad (3.6)$$

Where $Cp_{\max} = 0.593$

$$Tm = \frac{Pm}{\Omega} \quad (3.7)$$

Where Tm is mechanical torque.

Substitute equations 3.2 and 3.4 for equation 3.6. The torque becomes:

$$Tm = \frac{1}{2}\rho\pi R^3 Vv^2 \frac{Cp(\lambda,\beta)}{\pi} \quad (3.8)$$

The following equation illustrates the relationship between the power coefficient Cp and torque coefficient Ct.

$$Cp = \lambda Ct \quad (3.9)$$

Therefore, by substituting equation (3.9) into equation (3.8), the torque equation becomes(Manyonge et al., 2012):

$$Tm = \frac{1}{2}\rho\pi R^3 Vv^2 Ct \quad (3.10)$$

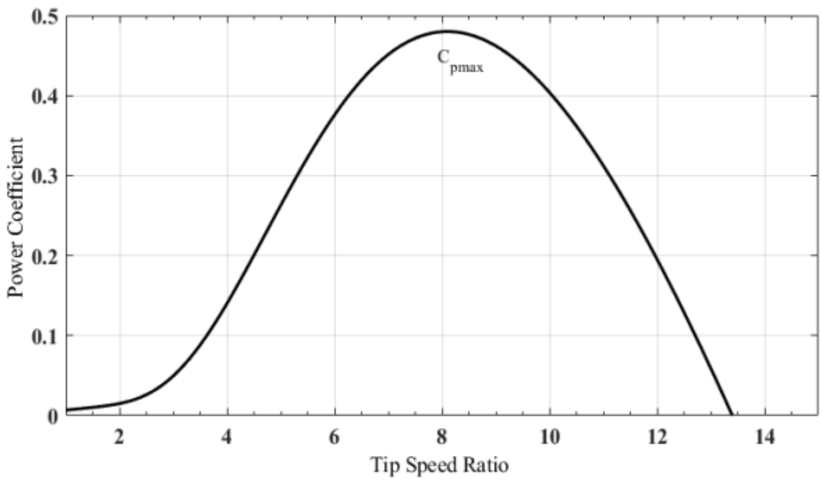

Figure 3. 5 Relationship between power coefficient and tip speed ratio(Jayathilake, 2017)

The rotor torque is obtained also from the rotational speed

$$T_m = \frac{P_m}{V_\omega} \quad (3.11)$$

Where pm, is mechanical power, Tm is mechanical torque

3.5. Mathematical Modelling of PMSG

Three-phase machine performance and behavior are usually defined and evaluated using the voltage and current equations. Except in situations in which a static rotor is present, the differential equations' coefficients that describe the dynamic behavior of the machines are time-varying. Such a system is challenging to mathematically represent because of the system's relative motion, which causes the flux connections, currents, and induced voltages to fluctuate constantly. By decoupling or separating the variables and solving equations including time-varying values by referring the full set of variables to a common reference frame that may be rotational or stationary, mathematical transformations are typically used to analyze complex electrical machinery. The Park transformation and the Clarke transformation are the two most well-known transformation methods. The machine's mathematical model's complexity can be(Hasoun et al., 2019)(Journal, 2015). The three-phase values (v_a, v_b, v_c) may be changed into the voltages v_d *and* v_q that the two-axis PMSG model requires(Zhang & Shu, 2010)

Park Transformation

Park's transformation is utilized to convert the three-phase voltages to (d,q) voltages. and described in equation 3.12:

$$\begin{bmatrix} V_d \\ V_q \\ V_0 \end{bmatrix} = \begin{bmatrix} \cos(\theta) & \cos(\theta - \frac{2\pi}{3}) & \cos(\theta + \frac{2\pi}{3}) \\ -\sin(\theta) & -\sin(\theta - \frac{2\pi}{3}) & -\sin(\theta + \frac{2\pi}{3}) \\ \frac{1}{2} & \frac{1}{2} & \frac{1}{2} \end{bmatrix} \begin{bmatrix} V_a \\ V_b \\ V_c \end{bmatrix} \tag{3.12}$$

The Clark inverse is given by

$$\begin{bmatrix} V_a \\ V_b \\ V_c \end{bmatrix} = \begin{bmatrix} \cos(\theta) & -\sin(\theta) & 1 \\ \cos(\theta - \frac{2\pi}{3}) & -\sin(\theta - \frac{2\pi}{3}) & 1 \\ \cos(\theta + \frac{2\pi}{3}) & -\sin(\theta + \frac{2\pi}{3}) & 1 \end{bmatrix} \begin{bmatrix} V_d \\ V_q \\ V_0 \end{bmatrix} \tag{3.13}$$

Where V_0 (zero-voltage component) is often ignored, and θ denotes the phase (a) electrical angle respect to the reference frame.

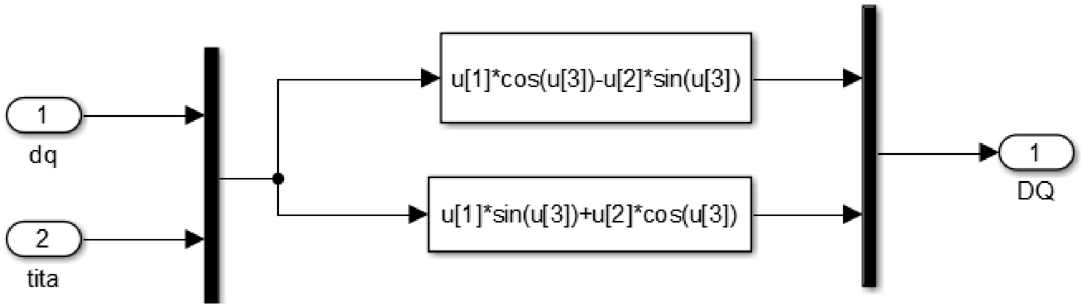

Figure 3. 6 Parks transformation in Simulink block

3.5.1 Tow-Axis Model of PMSG (DQ-axis Model)

To create permanent magnet synchronous Generator control, a mathematical model of the PMSG is required. It is rare for control design to employ the mathematical model of a 3-phase system. The time-varying model is the term used for this technique. Consequently, it becomes much harder to establish a control strategy.(Jaber & Abdulhasan, 2022). The permanent magnet synchronous generator mathematical model typically includes stator flux equations, voltage equations, mechanical equations, and electromagnetic torque equations(Yu et al., 2017)(Singh et al., 2011).

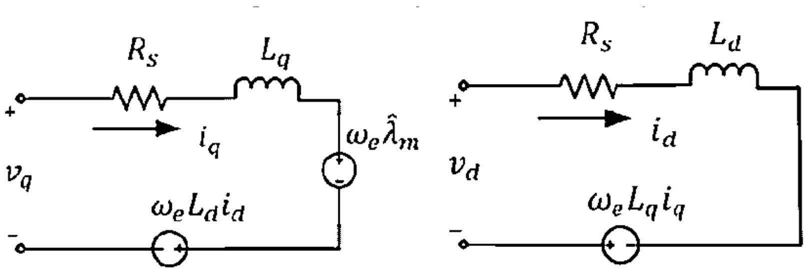

Figure 3. 7 . General dq-axis model of PMSG in the rotor field synchronous reference frame (Mahmoud et al., 2019)

The following assumptions were used to build the PMSG model without damper winding on the rotor reference frame(Madhu & Mathew, 2013)(Mahammadsoaib & Sajid, 2015)**.**

1. The EMF generated is sinusoidal.
2. Saturation is ignored.
3. No field current dynamics
4. Hysteresis losses and eddy current are ignored.

In the d-q coordinate system, the following equations may be expressed. In the rotor reference frame, the voltage formulas of the PMSG are shown(Mahammadsoaib & Sajid, 2015):

$$v_q = R_s i_q + \omega_r \lambda_d + \frac{d}{dt}\lambda_q \qquad (3.13)$$

$$v_d = R_s i_d - \omega_r \lambda_q + \frac{d}{dt}\lambda_d \qquad (3.14)$$

The flux linkage created is given by:

$$\lambda_q = L_q i_q \qquad (3.15)$$

$$\lambda_d = L_d i_d \qquad (3.16)$$

Substitute equations 3.15 and 3.16 into 3.13 and 3.14 respectively gives

$$v_q = R_s i_q + \omega_r \lambda_d + \frac{d}{dt} L_q i_q \qquad (3.17)$$

$$v_d = R_s i_d - \omega_r \lambda_q + \frac{d}{dt} L_d i_d \qquad (3.18)$$

The electromagnetic torque for PMSG in the (d-q) axes may be calculated using equation 3.19(Mahammadsoaib & Sajid, 2015):

$$T_e = \frac{3}{2}\frac{p}{2}(\lambda_d i_d - \lambda_q i_q) \qquad (3.19)$$

The equation that represents the mechanical torque is given as(Mahammadsoaib & Sajid, 2015)(Meghni et al., 2017):

$$\omega_m = \int \frac{T_e - T_L - B\omega_m}{J} dt \qquad (3.20)$$

And mechanical speed of the PMSG generator can be represented as

$$\omega_m = \frac{2}{p}\omega_r \qquad (3.21)$$

Where Rs Stator resistance

Ld, The inductances on d-q axis

Te, Electromagnetic, and load torques

id, The stator currents on the d-q axis

ωr Electrical speed

Vd, The stator voltages on d-q axis

λd, The flux linkages of the stators on d-q axis.

P Number of poles

ωm Mechanical speed

J Moment of inertia

B Fraction factor

3.6 Mathematical Modelling of Grid Side and Machine Side Converter

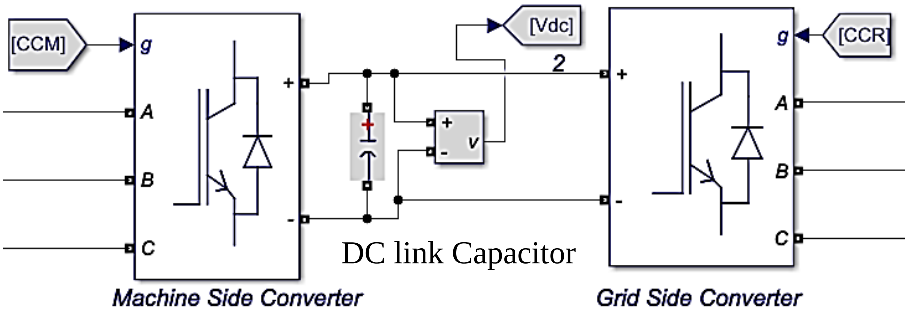

Figure 3. 8 Simulink model for Machine side and Grid side converter

3.6.1 Machine Side Converter (MSC) Modelling

Designing a machine-side converter for a wind farm using a PMSG involves mathematical modeling to understand and optimize the system's performance. The process typically includes modeling the PMSG, the power converter, and the control system.

The power converter typically involves power electronic devices like an Insulated Gate Bipolar Transistor (IGBT). The converter equations depend on the specific topology used (e.g., voltage source converter, current source converter). For a voltage source converter, the equations can include the following:

The PMSG and MSC mathematical model is

$$\frac{di_{sd}}{dt} = -i_{sd}\frac{R_{sd}}{L_{sd}} + i_{sq}\frac{L_{sq}}{L_{sd}}n_p\omega i_{sq} + \frac{1}{L_{sd}}U_{sdc} - \frac{1}{L_{sd}}\varepsilon_{sd} \tag{3.25}$$

$$\frac{di_{sq}}{dt} = -i_{sq}\frac{R_s}{L_{sq}} - \frac{L_{sd}}{L_{sd}}n_p\omega i_{sd} - \frac{n_p\omega\psi}{L_{sq}} + \frac{1}{L_{sq}}U_{sq} - \frac{1}{L_{sq}}\varepsilon_{sq} \tag{3.26}$$

where U_{sd} and U_{sq} are the d-axis and q-axis stator armature voltages. i_{sd} and i_{sq} are the d-axis and q-axis components of stator currents. L_{sd} and L_{sq} are the d-axis and q-axis stator inductances. ω is the rotor speed. n_p Represents magnetic pole logarithms. R_s is the stator resistance. ψ represents the permanent magnet chain. In addition, the disturbance ε_{sd} and ε_{sq} vector represents model uncertainties including the external disturbances and the Pulse Width Modulation (PWM) offset. ε_{sd} and ε_{sq} were generally assumed to be bounded by D_{sd} and D_{sq}

$$\begin{aligned} |\varepsilon_{sd}| &\leq D_{sd} \\ |\varepsilon_{sq}| &\leq D_{sq} \end{aligned} \tag{3.26}$$

where D_{sd} and D_{sq} are the boundaries of ε_{sd} and ε_{sq}

3.6.2 Grid Side Converter Modelling and RL Filter

The two parts of the wind energy conversion system are linked with the two converters shown in Figure 3.9 the modeling of the second linkage is the grid side converter is described below.

Therefore, the grid-side dynamic model is given by

$$\frac{di_{gd}}{dt} = -i_{gd}\frac{R_c}{L_c} + i_{gq}\omega_q + \frac{1}{L_c}E_{gd} - \frac{1}{L_c}U_{gd} - \frac{1}{L_c}\varepsilon_{gd} \tag{3.28}$$

$$\frac{di_{gq}}{dt} = -i_{gq}\frac{R_c}{L_c} - i_{gd}\omega_g + \frac{1}{L_c}E_{gq} - \frac{1}{L_c}U_{gq} - \frac{1}{L_c}\varepsilon_{gq} \tag{3.29}$$

where U_{gd} and U_{gq} are the control voltages. i_{gd} and i_{gq} are the components of grid-side currents. ω_g is the power grid frequency. L_c and R_c are the filter inductance and resistance. E_{gd} and E_{gq} Express the d-axis and q-axis power grid potential components (usually, = 0). The and can be gotten by the voltage phase-locked loop. ε_{gd} and ε_{gq} are also the uncertainties and meet

$$\begin{aligned} |\varepsilon_{gd}| &\leq D_{gd} \\ |\varepsilon_{gd}| &\leq D_{gq} \end{aligned} \tag{3.30}$$

where D_{gd} and D_{gq} are the boundaries of ε_{gd} and ε_{gq}

The following two equations represent respectively the formulas relating to the active and reactive power

$$P = v_{gd} i_{gd} + v_{gq} i_{gq} \quad (3.31)$$

$$Q = v_{gq} i_{gd} - v_{gd} i_{gq} \quad (3.32)$$

3.7. Maximum Power Point Tracking (MPPT)

Maximum power tracking in wind turbines refers to the process of continuously adjusting the angle and speed of the turbine blades to ensure that the turbine extracts the maximum amount of power from the wind. In the context of a PMSG for wind energy generation, you can use various mathematical models to implement MPPT control. One common approach is the Perturb and Observe (P&O) algorithm. Two basic types of the mathematical model for MPPT using P&O for a PMSG-based wind energy system:

System Dynamics: Start with the basic equation governing the PMSG behavior. The dynamic equation of a PMSG can be represented as:

$$T_e = \frac{3}{2} P\left(\frac{V_d i_q - V_q i_d}{\omega_r}\right) \quad (3.22)$$

Where: T_e is the electromagnetic torque.

P is the number of pole pairs.

V_d and V_q are the d- and q-axis stator voltages, respectively.

i_d and i_d are the d- and q-axis stator currents, respectively.

ω_r is the rotor speed.

The Perturb and Observe (P&O) algorithm is a simple and widely used MPPT technique. The basic idea is to perturb the operating point and observe the change in power. Adjust the operating point in the direction of increased power.

$$P_{new} = V_{new} \cdot I_{new} \quad (3.23)$$

Compare P_{new} with the previous power P_{old} . If $P_{new} > P_{old}$, continue in the same direction; otherwise, change direction. (Sun et al., 2020).

To guarantee that the wind turbine rotates at its intended speed, the electromagnetic torque needs to be controlled, approximated using the MPPT approach, and then applied to the PMSG. Its optimum value exits $\beta = 0^o$ and the expression becomes as follows(Meghni et al., 2017)(Beltran et al., 2012)

$$T_{em\_ref} = P\frac{P_{terb\_ref}}{\Omega_t} = \frac{\rho \times \pi \times R^5 \times C_{p\_\max}(\lambda_{opt}) \times \Omega_{mec}^2}{2 \times \lambda_{opt}^3} \tag{3.24}$$

Then the pitch angle control of the turbine can be described in the following block diagram.

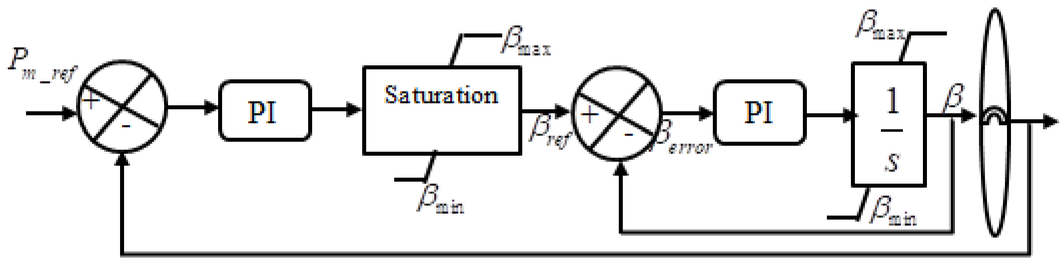

Figure 3. 9 Block diagram for Pitch angle control of wind turbine

3.8. Control of Wind Energy Integrated into the Grid

3.8.1 Control Strategy

The frequency converters, which are made up of a PWM inverter and a rectifier, must be controlled to modify the voltage, frequency, and active and reactive power injected into the grid when the wind speed varies.(Bossoufi et al., 2015; Jin et al., 2014; Johnson, 2001), to achieve the desired control objectives. As a result, the state vector and control vector are selected as described in eq 3.33 and 3.34:

$$[X] = [I_{sd}, I_{sq}, \Omega_{mec}, I_{gd}, I_{gq}] \tag{3.33}$$

$$[U] = [V_{sd}, V_{sq}, V_{fd}, V_{fq}] \tag{3.34}$$

3.8.2 Slide Mode Controller Design

In general, the goal of sliding mode control is to make the system slide along the preplanned sliding mode surface in a finite amount of time and remain there in the face of uncertainties, such as wind speed uncertainties or system parameter uncertainties, if the system is dynamic. With the latter, the system can be configured to switch between differentiators at any time by utilizing a discontinuous control signal structure. In this case, the system dynamic combines the beneficial properties of each of these structures to achieve the desired system behavior(Rhaili et al., 2020) (Yin et al., 2015). However, the ordinary SMC suffers from chattering and reaching the phase instability problem(Freire et al., 2012)(Mousa et al., 2020). Therefore, an SMC control strategy has been proposed to solve the common SMC problems and improve the system's performance(Jin et al., 2014; Johnson, 2001). This technique is characterized by its simplicity and efficiency.

In the proposed SMC control scheme, the chosen sliding surface is as follows(Majout et al., 2022):

$$S(X) = \left(\frac{d}{dt} + \delta \right)^{n-1} \times e(x) \tag{3.35}$$

where n denotes the order of the system, d is a positive constant, and $e(x)$ is the error between the desired signal x_{ref} and the state variable x. The tracking error dynamics of the suggested sliding surface become as follows when n = 1 is selected:

$$S(X) = e(x) = x_{ref} - x \tag{3.36}$$

Furthermore, the first-order SMC includes two terms (U_{eq} and U_n), where Ueq is an equivalent control that characterizes the system's behavior on the sliding surface, whereas U_n is a switching control based on a discontinuous function (sign). It is employed to satisfy the condition of attractiveness and stabilization(Benamor et al., 2019)(Freire et al., 2012)(Mousa et al., 2019). Therefore, to attain commutation around the surface of PSMC, each component of the control approach is calculated as the addition of two terms(Yin et al., 2015)(Majout et al., 2022)(Rhaili et al., 2020), as follows:

$$U_c = U_{eq} \text{ and } U_n \tag{3.37}$$

$$U_n = K_n \operatorname{sgn}(S_n) \tag{3.38}$$

Where: K_n is a positive switching gain that is selected to attain the optimum performance and minimize the dynamic system disturbance. $\operatorname{sgn}(S_n)$ is a discontinuous mathematical function characterized by an imperfect switching that causes the control signal to chatter(González et al., 2010). A novel smooth continuous switching control has been presented to smooth the signal to lessen this problem. The principle of this technique is based on replacing the ordinary discontinuous function (Sign) in the switching control with a smooth continuous function as described in equation 3.37(González et al., 2010)(Karim et al., 2016):

$$U_n = K_n \times Smooth(S_n) \tag{3.39}$$

where $Smooth(S(X))$ is a smooth continuous function defined by the following:

$$Smooth(\lambda', S) = \frac{\lambda' S}{|\lambda' S| + \varepsilon} \tag{3.40}$$

ε is a small positive of the boundary layer width and λ' is a positive constant used to adjust the tuning rate of the function. These two parameters (ε, λ') determine the steepness of the continuous function. Moreover, the state-dependent boundary layer ε is designed as follows:

$$\varepsilon = (1 - |Smooth(\lambda', S)| + \delta_1) \tag{3.41}$$

where δ_1 is a small positive constant.

3.8.2.1 Machine Side Control

On this side, three controllers, using the sliding mode, are designed to control the direct and quadrature current components of the stator (I_{sd}, I_{sq}) and the speed (Ω_{mec}).The-sliding surfaces have been fixed as follows(Aroussi et al., 2020b):

$$S(I_{sd}) = e(I_{sd}) = I^*_{sd} - I_{sd} \tag{3.42}$$

$$S(I_{sq}) = e(I_{sq}) = I^*_{sq} - I_{sq} \tag{3.43}$$

$$S(\Omega_{mec}) = e(I\Omega_{mec}) = \Omega^*_{mec} - \Omega_{mec} \tag{3.44}$$

where I^*_{sd}, I^*_{sq} are the references of the direct and the quadrature stator current, respectively,

and Ω^*_{mec} is the mechanical speed reference.

Applying the time derivative to $S(I_{sd})$, $S(I_{sq})$ and $S(\Omega_{mec})$, the resulting equations are as follows:

$$\dot{S}(I_{sd}) = \dot{I}^*_{sd} + \frac{R_s}{L_d} \times I_{sd} - \omega_e \times \frac{L_q}{L_d} \times I_{sq} - \frac{V_{sd}}{L_d} \tag{3.45}$$

$$\dot{S}(I_{sq}) = \dot{I}_{sq}^{*} + \frac{R_s}{L_q} \times I_{sq} + \omega_e \times \frac{L_d}{L_q} \times I_{sd} + \omega_e \times \frac{\varnothing f}{L_q} - \frac{V_{sq}}{L_q} \tag{3.46}$$

$$\dot{S}(\Omega_{mec}) = \dot{\Omega}_{mec}^{*} + \frac{f}{J_{tot}} \times \Omega_{mec} + \frac{\mu}{J_{tot}} \times I_{sq} - \frac{1}{J_{tot}} \times T_{turbine} \tag{3.47}$$

With $\mu = \frac{3}{2} \times P \times \varnothing_f$ the sliding mode occurs on the sliding surface when the invariance conditions of the sliding surface are ensured, ($\dot{S}(X) = 0$) and_$V_{sd,qN} = 0$(Hammoumi et al., 2019). Hence, the equivalent control expression V_{sd,q_eq} for each axis is derived from Equations (44) and (46). gives,

$$V_{sd\_eq} = L_d \left[\dot{I}_{sd}^{*} + \frac{R_s}{L_d} \times I_{sd} - \omega_e \times \frac{L_q}{L_d} \times I_{sq} \right] \tag{3.48}$$

$$V_{sq\_eq} = L_q \left[\dot{I}_{sq}^{*} + \frac{R_s}{L_d} \times I_{sq} + \omega_e \times \frac{L_d}{L_q} \times I_{sd} + \omega_e \times \frac{\varnothing_f}{L_q} \right] \tag{3.49}$$

Whereas the switching control expressions V_{sd_N}, V_{sq_N} are defined as follows:

$$V_{sd\_N} = K_d \times Smooth(S(I_{sd})) \quad \text{with } K_d > 0 \tag{3.50}$$

$$V_{sq\_N} = K_q \times Smooth(S(I_{sq})) \quad \text{with } K_q > 0 \tag{3.51}$$

From the expression in equations 3.48 to 3.51, the overall control expression can be written as:

$$V_{sd\_ref} = V_{sd\_eq} + V_{sd\_N} \tag{3.52}$$

$$V_{sq\_ref} = V_{sq\_eq} + V_{sq\_N} \tag{3.53}$$

By using equations 3.52 and 3.53, the controller design of the generator side converter can be formed as follows:

$$V_{sd\_ref} = L_d \left[\dot{I}_{sd}^{*} + \frac{R_s}{L_d} \times I_{sd} - \omega_e \times \frac{L_q}{L_d} \times I_{sq} \right] + K_d \times Smooth(S(I_{sd})) \tag{3.54}$$

$$V_{sq\_ref} = L_q\left[\dot{I}^*_{sq} + \frac{R_s}{L_d}\times I_{sq} + \omega_e \times \frac{L_d}{L_q}\times I_{sd} + \omega_e \times \frac{\varnothing_f}{L_q}\right] + K_q \times Smooth(S(I_{sq})) \qquad (3.55)$$

Similarly, the machine-side converter current control is

$$I^*_{sq} = I_{sq\_eq} + I_{sq\_N} \qquad (3.56)$$

With each component as :

$$\begin{cases} I_{sq\_eq} = -\frac{J_{tot}}{\mu}\left[\dot{\Omega}^*_{mec} + \frac{f}{J_{tot}}\times\Omega_{mec} - \frac{1}{J_{tot}}\times T_{turbine}\right] \\ I_{sq\_N} = K_{\Omega_{mec}} \times Smooth(S(\Omega_{mec})) \text{ with } K_{\Omega_{mec}} > 0 \end{cases} \qquad (3.57)$$

3.8.2.2 Grid Side Converter (GSC) Control

To keep the DC-link voltage at a constant value, a PI controller was applied to regulate the voltage measured V_{DC} to track its reference V_{DC_ref} . Furthermore, to adjust the grid current frequencies and reach a unit power factor(Aroussi et al., 2020a),two controllers using the sliding mode are designed to control the direct and quadrature current components (I_{gd},I_{gq}) of the GSC, as shown in Figure 3.10.

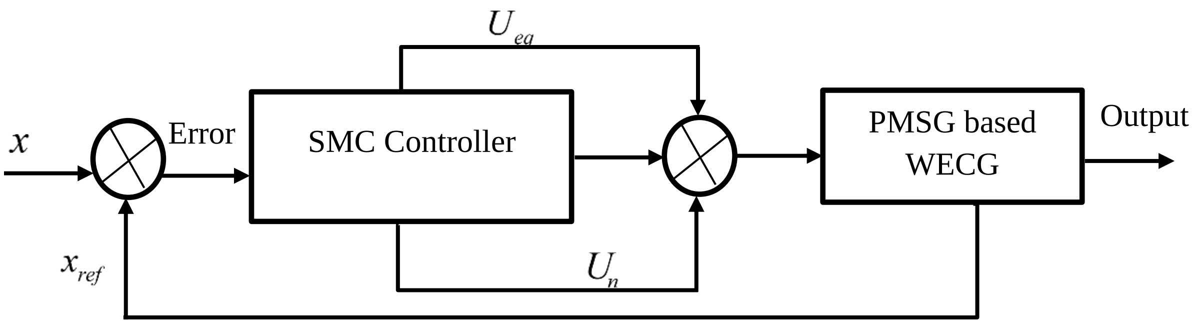

Figure 3. 10. General block diagram for grid side control

On this side, the sliding surfaces have been fixed as follows:

$$S(I_{gd}) = e(I_{gd}) = I^*_{gd} - I_{gd} \qquad (3.58)$$

$$S(I_{gq}) = e(I_{gq}) = I^*_{gq} - I_{gq} \qquad (3.59)$$

I^*_{gd}, I^*_{gq} are references to the quadrature and direct grid currents. Using the same methodology as the MSC control once more, the grid-side converter's controller will be designed as follows:

$$V_{fd\_ref} = V_{fd\_eq} + V_{fd\_N} \tag{3.60}$$

$$V_{fq\_ref} = V_{fq\_eq} + V_{fq\_N} \tag{3.61}$$

$$\begin{cases} V_{fd\_eq} = L_f \left[\dot{I}^*_{gd} + \dfrac{R_f}{L_f} \times I_{gd} - \omega_g \times I_{gq} + \dfrac{V_{gd}}{L_f} \right] \\ V_{fd\_N} = K_{fd} \times Smooth(S(I_{rd})) \quad \text{with } K_{fd} > 0 \end{cases} \tag{3.62}$$

$$\begin{cases} V_{fq\_eq} = L_f \left[\dot{I}^*_{gq} + \dfrac{R_f}{L_f} \times I_{gq} + \omega_g \times I_{gd} + \dfrac{V_{gq}}{L_f} \right] \\ V_{fq\_N} = K_{fq} \times Smooth(S(I_{rq})) \quad \text{with } K_{fq} > 0 \end{cases} \tag{3.63}$$

where I^*_{gq} is produced by the reactive power Q_{g_ref} that is fixed to zero to reach the unity power factor control, while I^*_{gd} is generated by the DC-link voltage regulator.

3.8.3 Stability Analysis

The global stability condition of the proposed SMC for the machine side converter and grid side converter, the Lyapunov stability function is introduced as follows(Karaoui et al., 2022; Mahfoud et al., 2021; Majout et al., 2021):

$$\begin{cases} V_{MSC} = \dfrac{1}{2}\left(S^2_{I_{sd}} + S^2_{I_{sq}} + S^2_{\omega_{mec}}\right) \\ V_{GSC} = \dfrac{1}{2}\left(S^2_{I_{gd}} + S^2_{I_{gq}}\right) \end{cases} \tag{3.64}$$

where the Lyapunov stability function V_{MSC} is chosen for the MSC, while V_{GSC} VGSC is selected for the grid-side converter.

If the Lyapunov function derivative is negative, the sliding mode stability is guaranteed.

$$\begin{cases} V_{MSC} < 0 \\ V_{GSC} < 0 \end{cases} \tag{3.65}$$

BY taking the first derivative of V_{MSC} and V_{GSC} in equation 3.63 for time can be described as follows:(Karaoui et al., 2022; Majout et al., 2021):

$$\begin{cases} \dot{V}_{MSC} = S_{I_{sd}} \times \dot{S}_{I_{sd}} + S_{I_{sq}} \times \dot{S}_{I_{sq}} + S_{\omega_{mec}} \times \dot{S}_{\omega_{mec}} \\ V_{GSC} = S_{I_{gd}} \times \dot{S}_{I_{gd}} + S_{I_{gq}} \times \dot{S}_{I_{gq}} \end{cases} \tag{3.66}$$

When each derivative surface $\dot{S}(X)$ replaces equations 3.45-3.47 and 3.62-3.63 in equation 3.66 then the final surface equation becomes

$$\begin{cases} \dot{V}_{MSC} = S_{I_{sd}} \times (\dot{I}^{*}_{sd} + \frac{R_s}{L_d} \times I_{sd} - \omega_e \times \frac{L_q}{L_d} \times I_{sq} - \frac{V_{sd}}{L_d}) + S_{I_{sq}} \times (\dot{I}^{*}_{sq} + \frac{R_s}{L_q} \times I_{sq} + \omega_e \times \\ \qquad \frac{L_d}{L_q} \times I_{sd} + \omega_e \times \frac{\varnothing f}{L_q} - \frac{V_{sq}}{L_q}) + S_{\omega_{mec}} \times (\dot{\Omega}^{*}_{mec} + \frac{f}{J_{tot}} \times \Omega_{mec} + \frac{\mu}{J_{tot}} \times I_{sq} - \frac{1}{J_{tot}} \times T_{turbine}) \\ \dot{V}_{GSC} = S_{I_{gd}} \times (\dot{I}_{gd\_ref} + \frac{R_f}{L_f} \times I_{gd} - \omega_g \times I_{gq} + \frac{V_{gd}}{L_f} - \frac{V_{fd}}{L_f}) + S_{I_{gq}} \times \\ \qquad (\dot{I}_{gq\_ref} + \frac{R_f}{L_f} \times I_{gq} + \omega_g \times I_{gd} + \frac{V_{gq}}{L_f} - \frac{V_{fq}}{L_f}) \end{cases} \tag{3.67}$$

Then replace equations 3.55, 3.56,3.58 and 3.63 into equation 3.67 and the final equation becomes

$$\begin{cases} \dot{V}_{MSC} = -K_d \times S_{I_{sd}} \times Smooth(S(I_{sd})) - K_q \times S_{I_{sq}} \times Smooth(S(I_{sq})) \\ \qquad - K_{\omega_{mec}} \times S_{\omega_{mec}} \times Smooth(S(\omega_{mec})) \\ \dot{V}_{GSC} = -K_{fd} \times S_{I_{gd}} \times Smooth(S(I_{rd})) - K_{fq} \times S_{I_{gq}} \times Smooth(S(I_{rq})) \end{cases} \tag{3.68}$$

So the final expression of smooth(S(X)) become

$$\begin{cases} \dot{V}_{MSC} = -K_{\omega_{mec}} \times \left|S_{\omega_{mec}}\right| - K_d \times \left|S_{I_{sd}}\right| - K_q \times \left|S_{I_{sq}}\right| \\ \dot{V}_{GSC} = -K_{fd} \times \left|S_{I_{gd}}\right| - K_{fq} \times \left|S_{I_{gq}}\right| \end{cases} \tag{3.69}$$

From equation 3.69 $K_{\omega_{mec}} > 0, K_d > 0$ and $K_q > 0\,; V_{MSC} < 0$ and $K_{fd} > 0, K_{fq} > 0\,; V_{GSC} < 0$ from it is understood that the Lyapunov condition is satisfied, and the main objectives of the proposed control are achieved.

The overall model and control system for wind energy generation using PMSG and its MSC and GSC control mechanism are described in Figure 3.11.

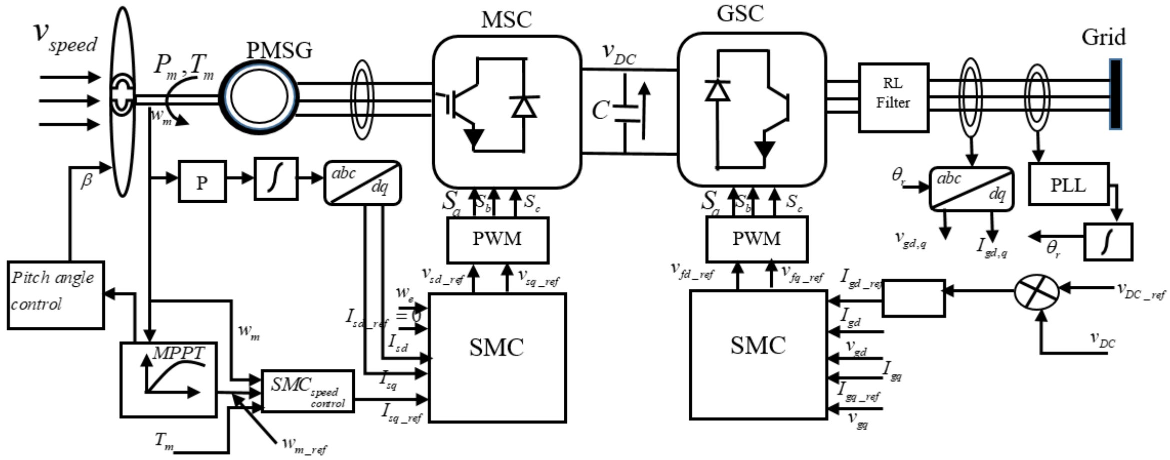

Figure 3. 11 . Overall block diagram of the system

3.9 RL Filter

In the context of wind farms and their integration into the electrical grid, Resistance-Inductance (RL) elements are often used in various components of the power system for control, protection, and filtering purposes. Key applications of RL elements in wind farm grids:

Grid-Side Converters: Wind turbines are connected to the electrical grid through power electronic converters. These converters often include RL filters to mitigate high-frequency harmonics and reduce the impact of switching transients. The inductance helps smooth the current waveform, and the resistance dampens oscillations.

Rotor-Side Converters: Some wind turbines use doubly-fed induction generators (DFIGs) with power converters on the rotor side. RL filters may be employed in the converter circuits to improve the performance of the generator, reduce harmonics, and provide better control of the turbine.

Fault Ride-Through (FRT) Systems: RL elements can be incorporated into the design of fault ride-through systems. These systems enable wind turbines to remain connected to the grid and ride through short-term voltage disturbances, such as faults.

Harmonic Filtering: Wind turbines, especially those with power electronics, can introduce harmonics into the grid. RL filters are used to filter out these harmonics, ensuring that the injected current into the grid is within acceptable limits and compliant with grid codes.

3.10. Overall System Software Simulation Modeling and Design

In this section, the simulation models of PMSG are presented. The simulation models are designed using MATLAB/SIMULINK 2021a. The model shown in Figure 3.12 contains the generator, power converters, wind turbine, transformer, and so on. The type of wind turbine employed is a variable-speed wind turbine with full-scale power converters commonly known as the permanent magnet synchronous generator. The specification of the generator (with a rated power of 1.5MW) used to run the model is obtained from the ADAMA-I wind farm. The back-to-back two-level PWM converter has two converters, one is connected to the machine side (MSC) and another is connected to the grid side (GSC). With a slide mode control method implemented the MSC is used to control the active and reactive power while the GSC is used to maintain a constant DC-link voltage. Its subsystem model is shown in Figure.B1, Figure.B2, and Figure.B3(Appendix).

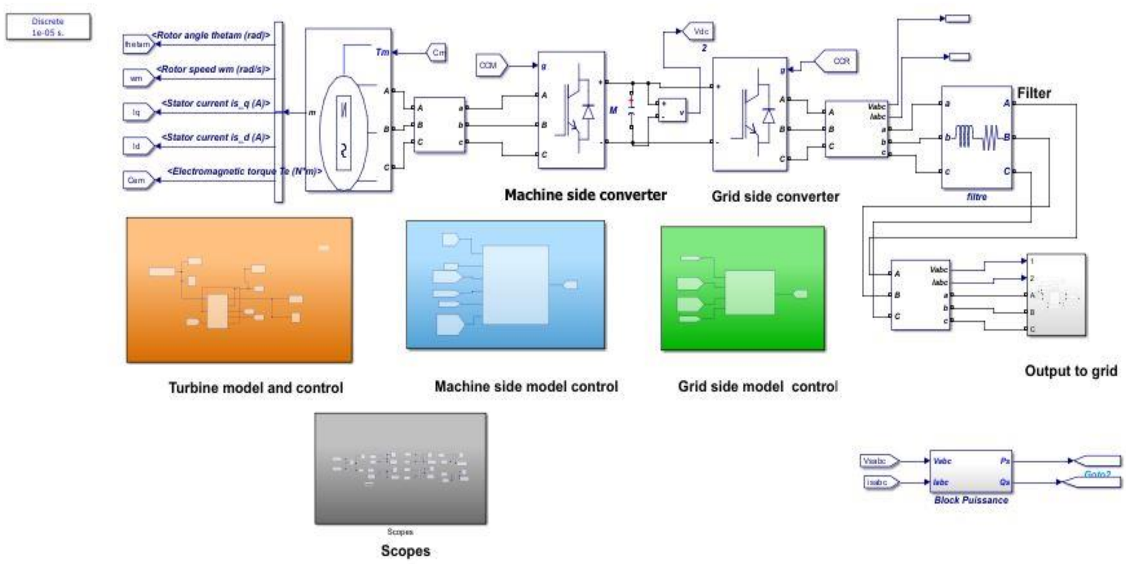

Figure 3. 12. Overall MATLAB Simulink model of the proposed system

CHAPTER FOUR

4. SIMULATION RESULT AND DISCUSSION

4.1 Introduction

In this chapter, the drive control system results of a permanent magnet synchronous generator for wind power generation integrated into the grid for power quality are discussed and analyzed. The simulation results describe the open loop and the controlled output variables. The nonlinear model of the PMSG is designed using the MATLAB/SIMULINK model. The sliding mode controller is used for the grid side and machine side converter to control the d-q current in SMC in PI controller mode.

4.2 Output Results without Control or Stability

4.2.1 Open Loop Output from Turbine

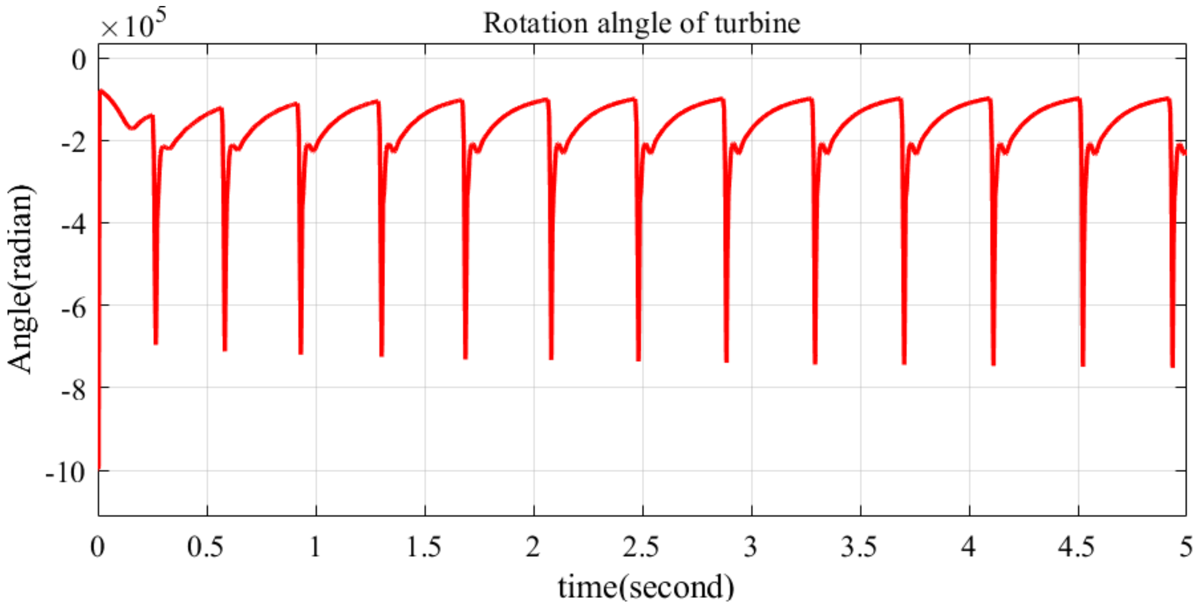

Figure 4. 1 Turbine rotation angle with wind direction

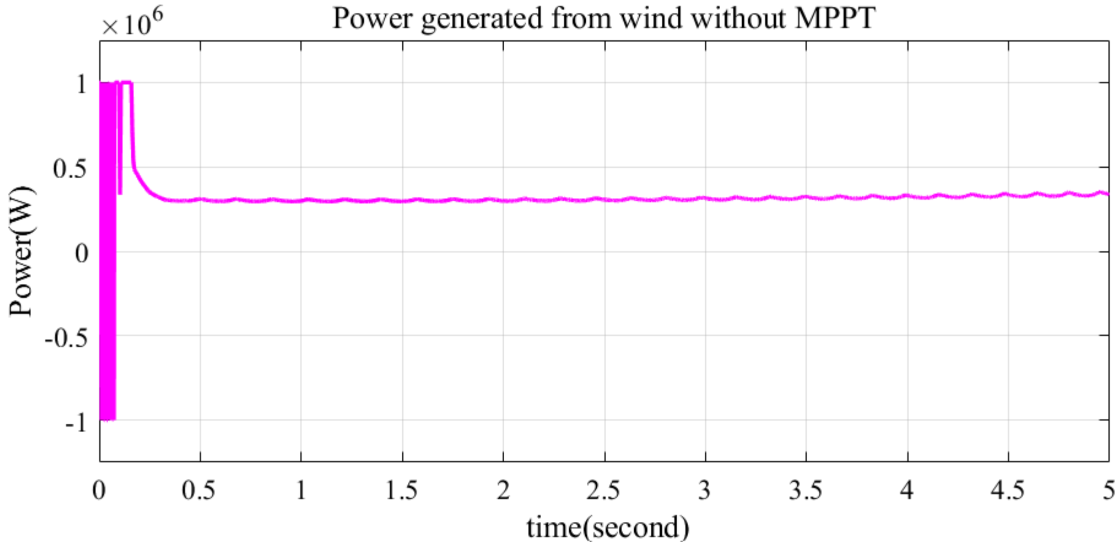

Figure 4. 2 Mechanical power generated from wind speed

Figures 4.1 and 4.2 are the outputs of the turbine of the wind generation system. The designed turbine rotation angle is described in Figure 4.1 as having the same frequency but it has a sharp corner in its rotation. In addition, the oscillation is not smooth since it has some sinusoidal without changing frequency. Figure 4.2 shows the power generated in the wind turbine speed or it is mechanical power. This power has fast oscillation up to some time even with different amplitudes. Figure 4.3 described below is the rotor speed of the PMSG without any control mechanism. As shown in the figure the speed signal at the start of the simulation is really unstable and oscillatory.

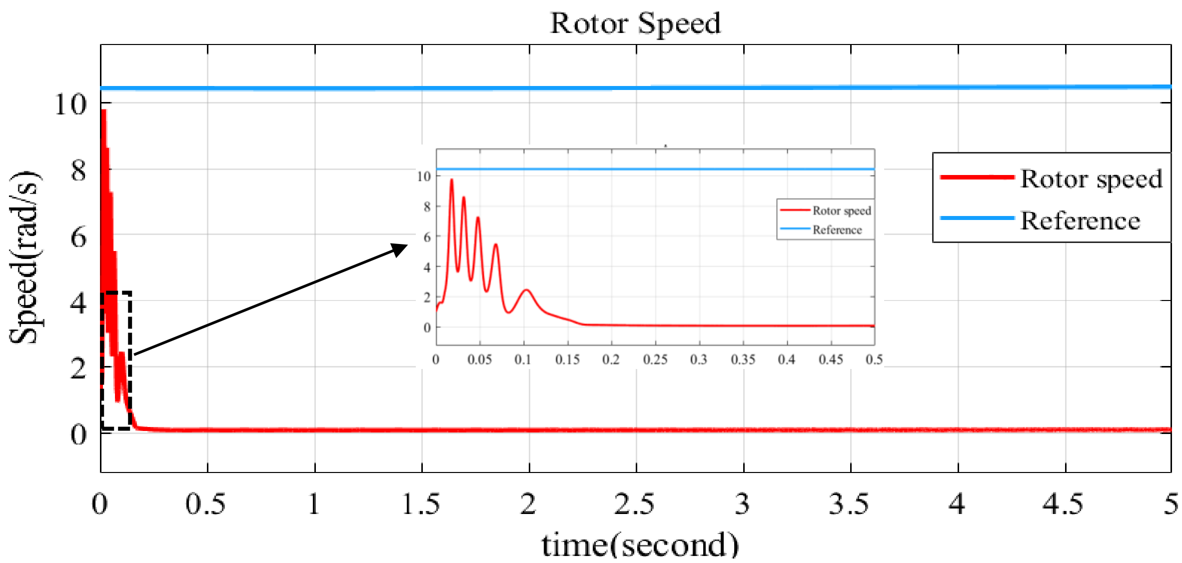

Figure 4. 3 Rotor speed of PMSG generator rotated with turbine speed

4.2.2 Open Loop Output from PMSG, Converters and Grids

Figures 4.4 and 4.5 below are the electromagnetic torque and power of the PMSG in an open loop mechanism or unstable mechanism. As shown in this figure the torque fluctuates back and forth in the sinusoid at the starting of the generator. This will create unstable power in the grid and cause power fluctuation.in proportion to the torque the power also fluctuates as shown in Figure 4.5. Due to this fluctuation of torque, the power is transient with different amplitude.

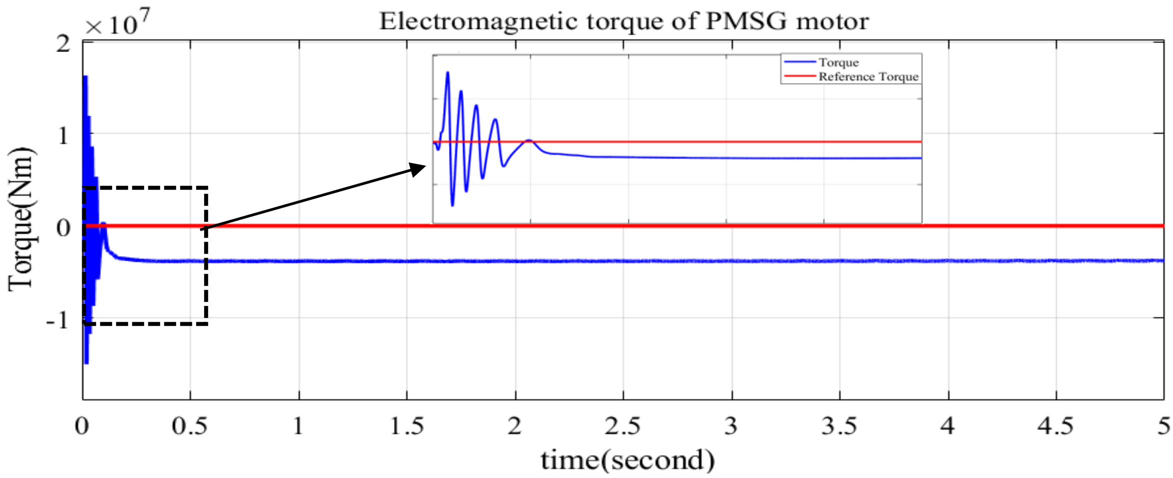

Figure 4. 4 Electromagnetic torque of PMSG

Figures 4.5 and 4.6 are the AC voltage and Current from the grid-side converter and grid-side DC voltage. Voltage and current at the start are very low and do have not the same amplitude of waves. This will create a harmonic distortion of the grid. The DC voltage in Figure 4.6 has an almost stable result but it still a smoothed signal.

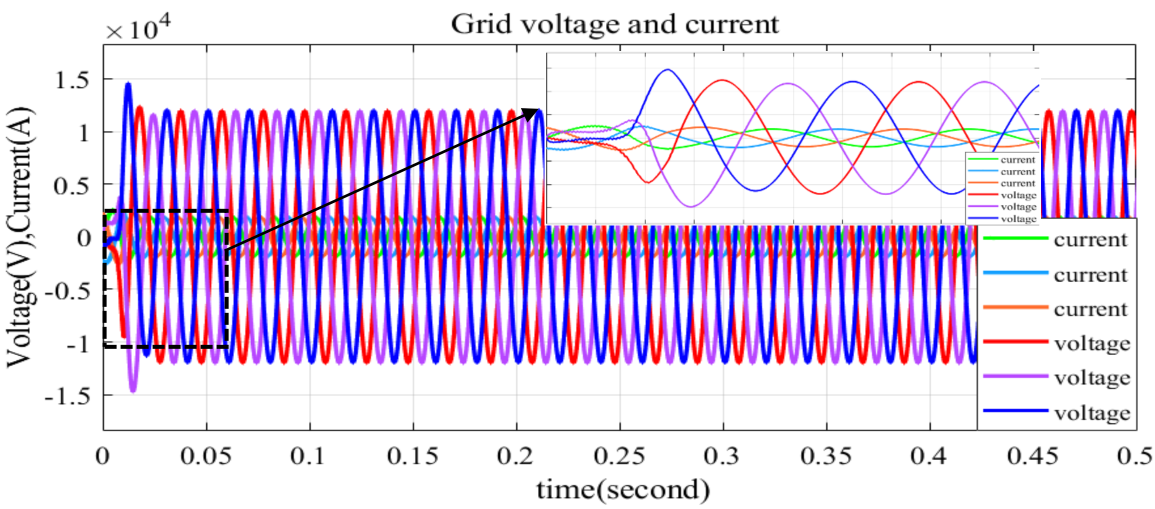

Figure 4. 5 Grid side voltage and current output

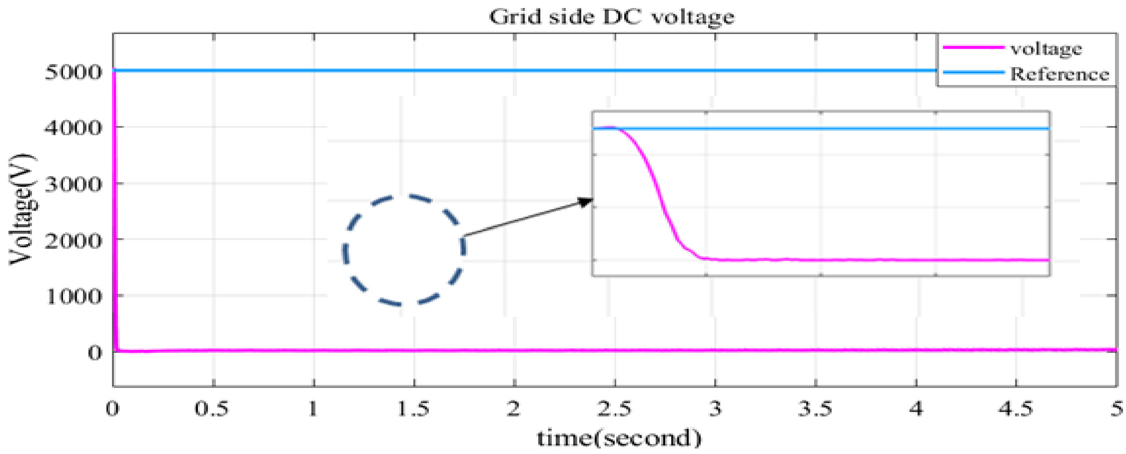

Figure 4. 6 Grid side DC voltage output

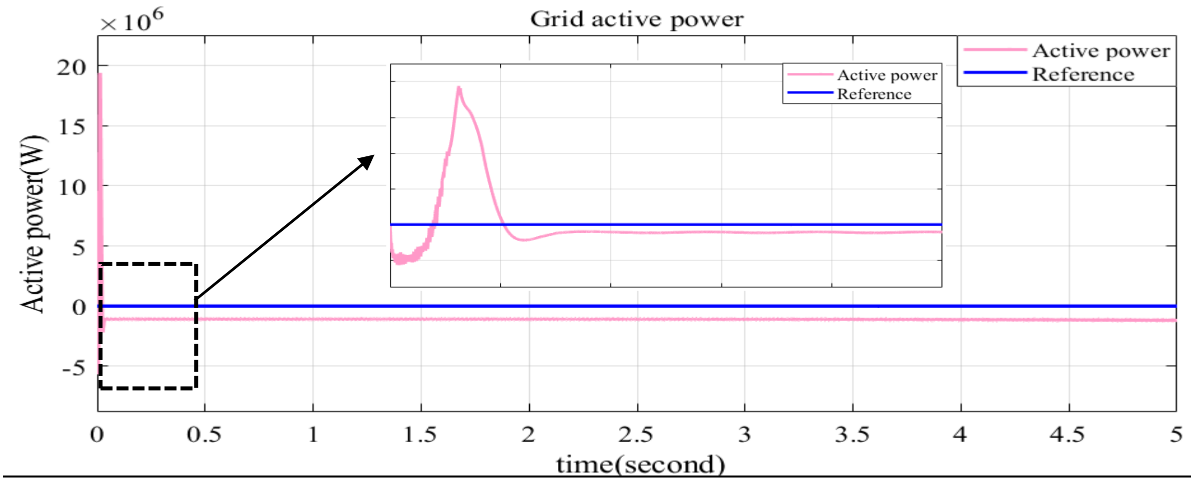

Figure 4. 7 Grid side Active power output

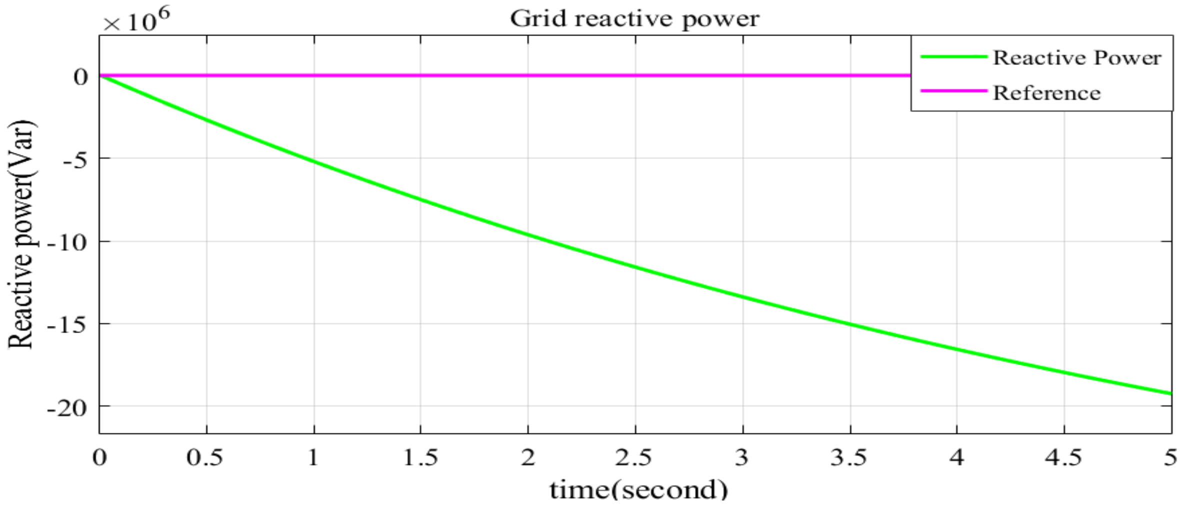

Figure 4.8 Grid side reactive power output

The grid's active and reactive power is shown in figures 4.7 and 4.8.from this figure it is clear that the active power is disturbed at the start of operation and it needs more time to back its stability. From Figure 4.8 the reactive power is increasing to the negative, this will reduce the power factor of the grid output. As shown from the zoomed view the active power follows the reference after some operation of the power system.

4.3. Output Results from Controller Stability

4.3.1 Controller Stable Output from Turbine

In this thesis, the stability of the power system from wind which is connected to the grid system becomes stable by using PI form sliding mode controller for PMSG motor and its converters.SMC is selected since the PMSG has no stator winding and its rotor is connected to the stator with internal winding.

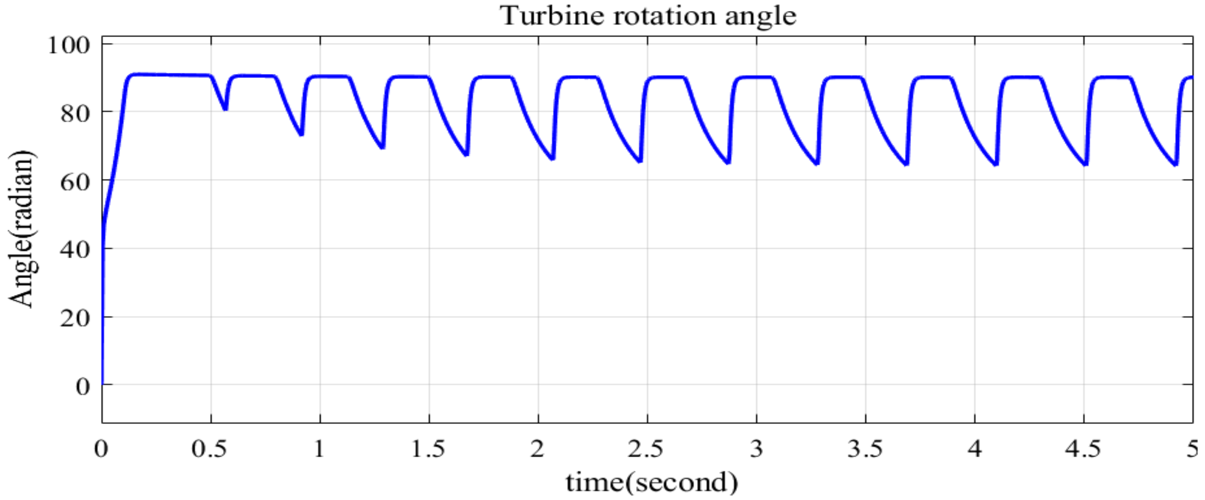

Figure 4. 9 Turbine rotation angle with wind direction

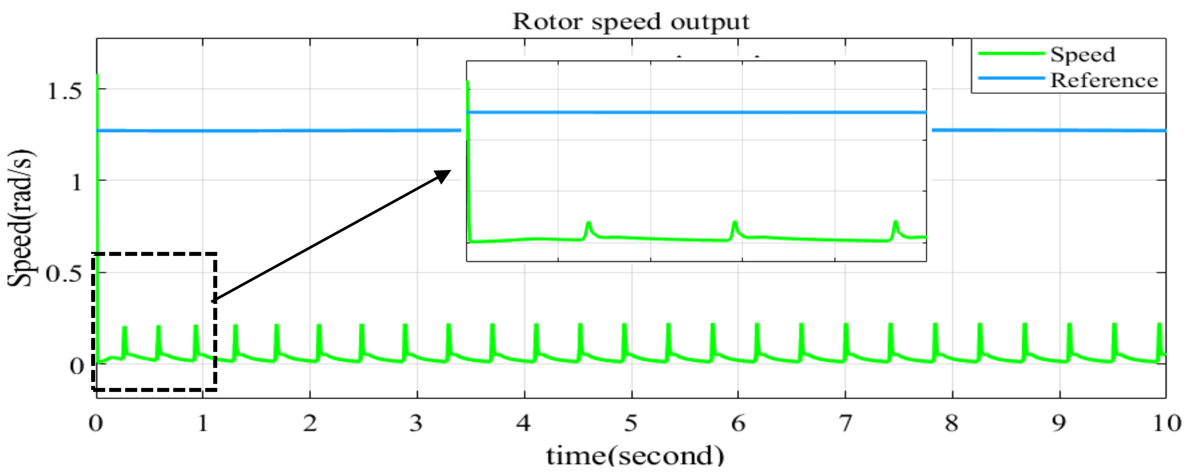

Figure 4. 10 Rotor speed output of PMSG

Figures 4.9 and 4.10 are the rotational angle of the turbine and rotor speed corresponding with the turbine rotation. From this figure 4.9, the angle is exactly controlled and has a specific boundary. The rotation angle does not vary with time which makes the PMSG rotate in equal frequency in time. This will create a smooth rotation of the motor and produce a stable power system from the wind. Due to the stability of the rotation angle, the speed described in Figure 4.10 is also stable and it follows the reference speed in equal frequency corresponding to time. These both show the effective control of the generator that leads to generating stable power.

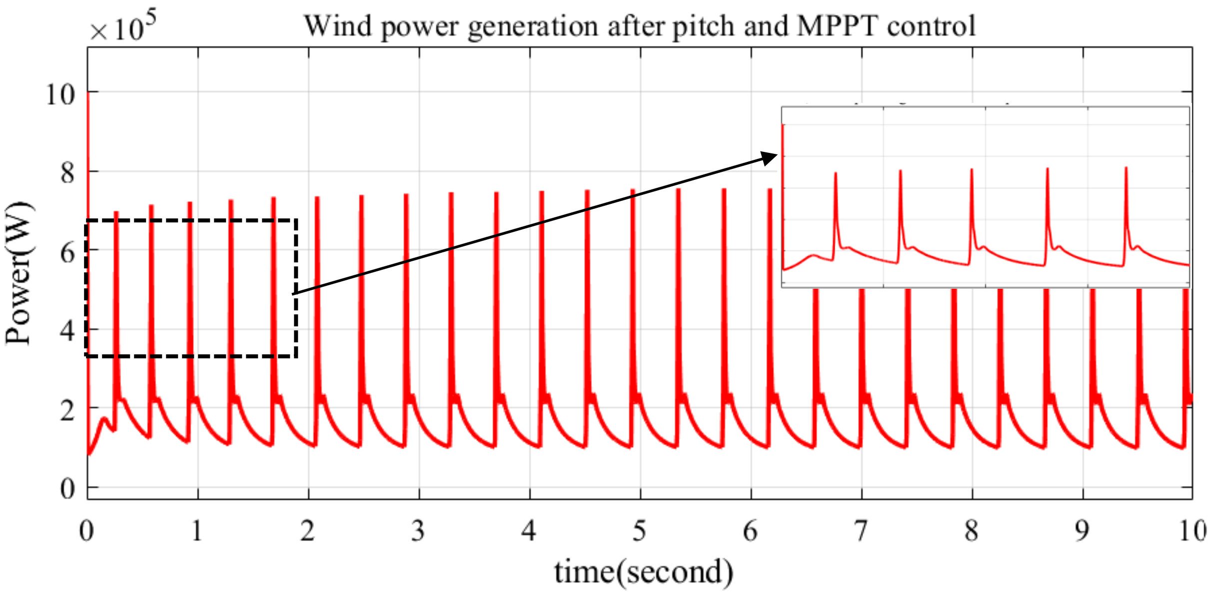

Figure 4. 11 Mechanical power generated from wind speed

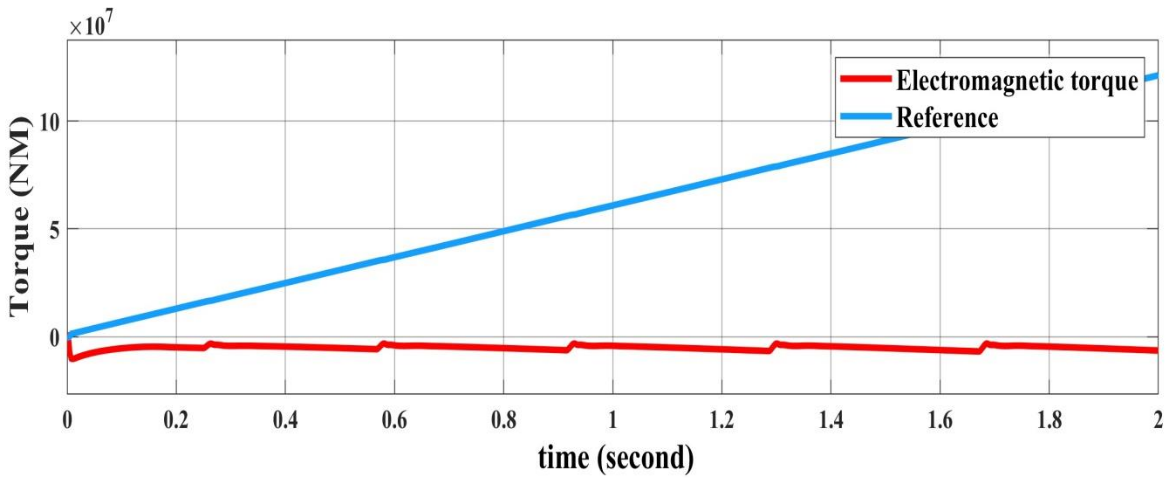

Figure 4. 12 Electromagnetic torque for PMSG

Figure 4.11 above is the mechanical power generated by wind. This power has an equal generating cycle without, distortion, and harmonics. This shows that the angle of rotation and speed of the generator are controlled in a good way. In addition to the power, the torque in Figure 4.12 also becomes very stable after controlling the motor. As shown in the pink line the torque has no increasing value concerning the reference torque. Throughput the running time of the motor the torque has equal value. This makes the generator smooth rotation and generates stable power with increasing power factor.

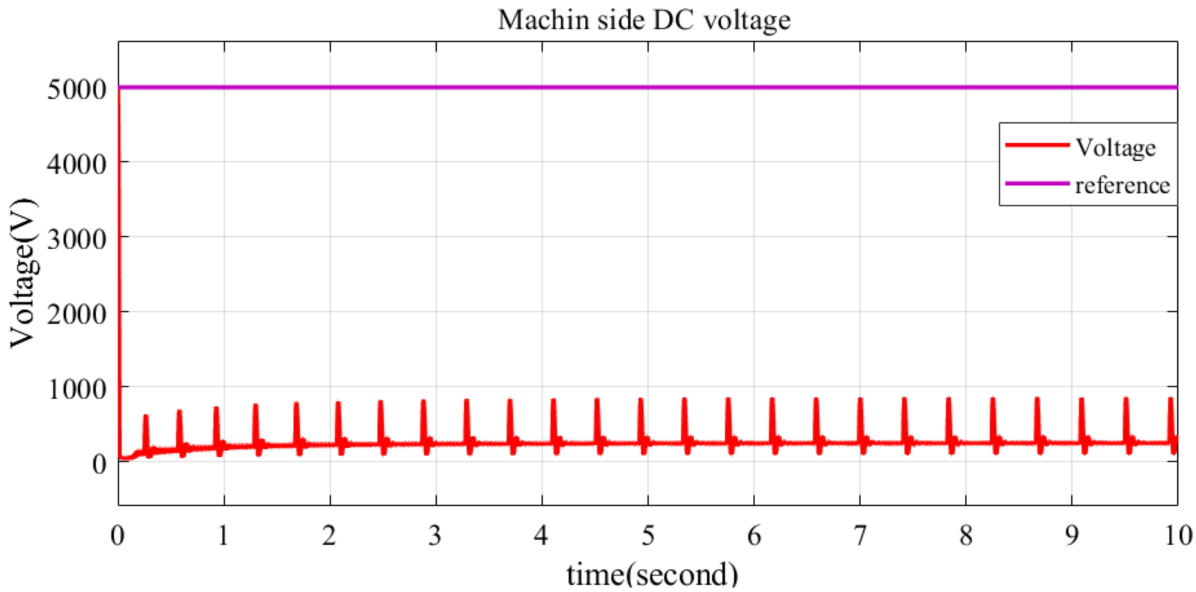

Figure 4. 13 Machine-side DC voltage output

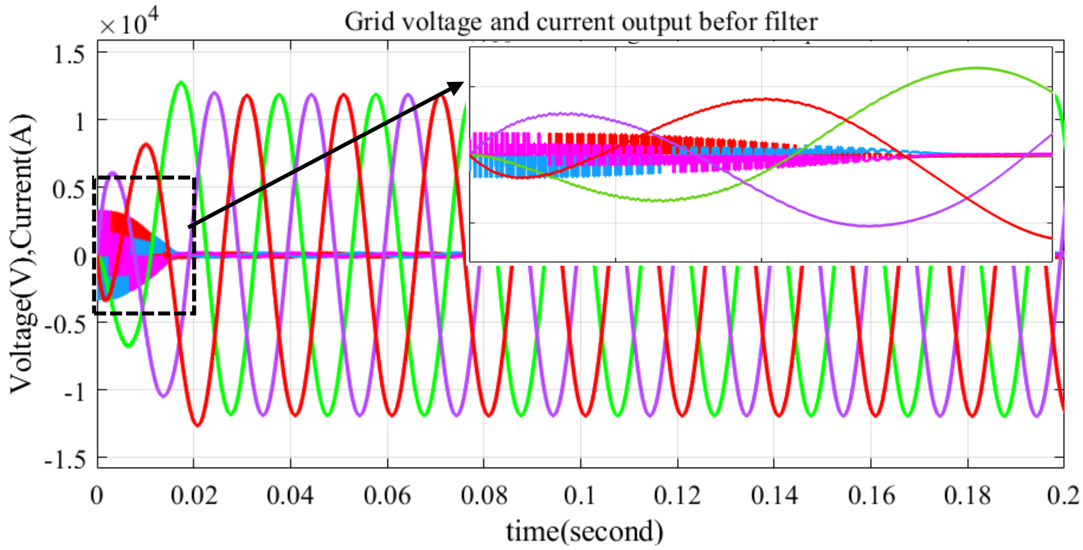

Figure 4. 14 Grid side voltage and current before the filter

Figure 4.14 below shows the current and voltage output after the grid converter without a filter. from this signal, it is understood that the voltage with higher amplitude has smooth and stable sinusoidal output. but the current shown in small amplitude with a zoomed view has a high starting current and also there are some harmonics in the current. After some time the current flows in a stable and equal amplitude signal. the harmonic signal from the current will create distortion and fluctuation in power stability.

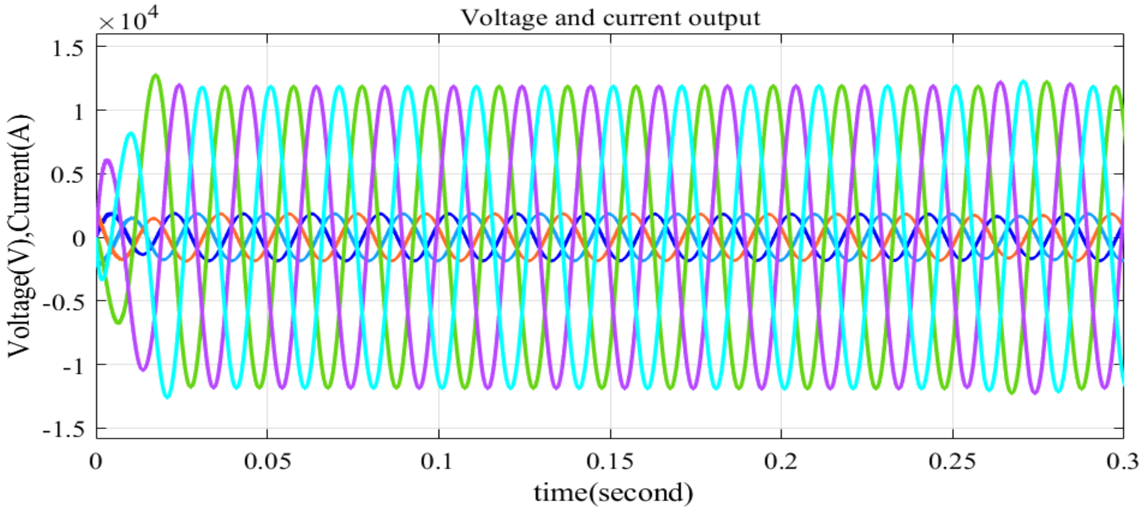

Figure 4. 15 Grid side voltage and current after filter

The signal described in Figure 4.15 above is the voltage and current after the addition of the filter. The main purpose of a filter is to remove unnecessary signals and harmonics, which are uncontrolled, signals. From this figure compared to figure 4.14 the voltage output is almost the same as figure 4.15.but the current in figure 4.15 is very stable and there are no harmonics compared with figure 4.14. this shows that the filter is important to remove and filter the uncontrolled signals and harmonics.

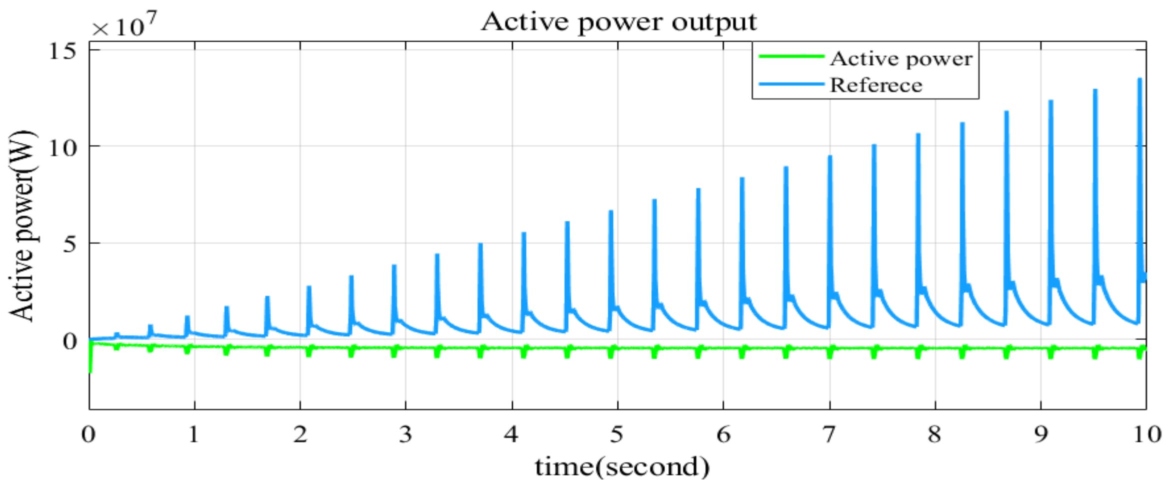

Figure 4. 16 Active power output from Grid

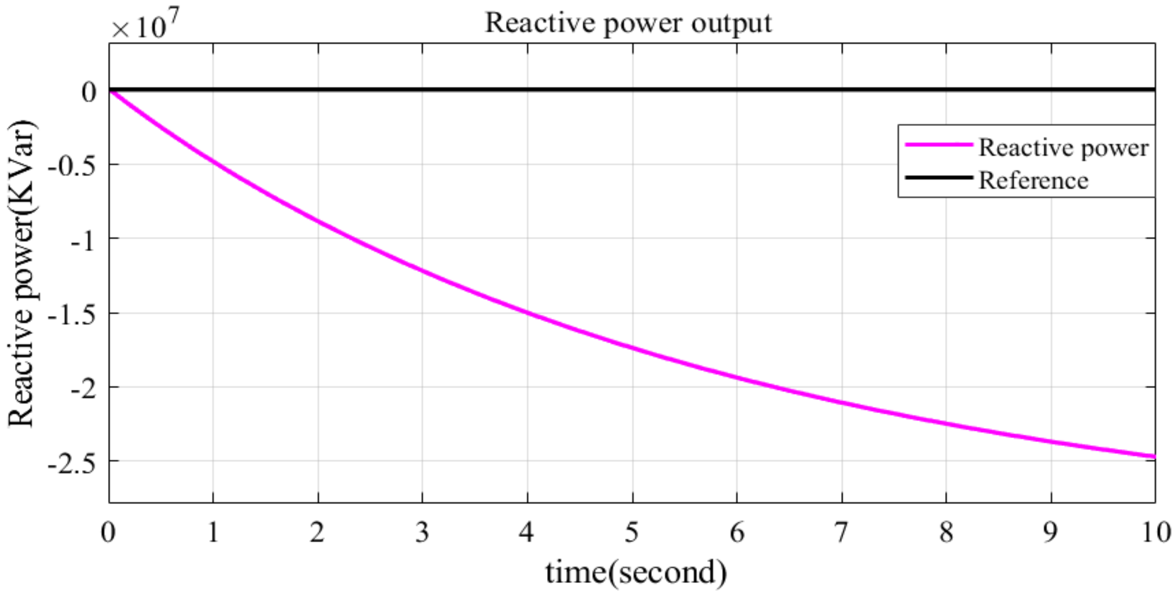

Figure 4. 17 Reactive power output from Grid

Figure 4.17 shows the reactive power output of the grid from the filter. The active power after control and filters is very stable and moves in equal amplitude as compared with that of the reference power. The stability of active power shows that all other parameters in the wind generation system are controlled and operated in stable conditions. As described in the reference power the amplitude of the reference power is increasing but the grid active power is operating in constant amplitude and frequency. Constant frequency operation of the grid system will lead to the stable operation of the whole system with our distortion. in another case, the figure shown in 4.17 is the reactive power of the grid-connected system. The reactive power is also stable and reduced to the constant after some time later.

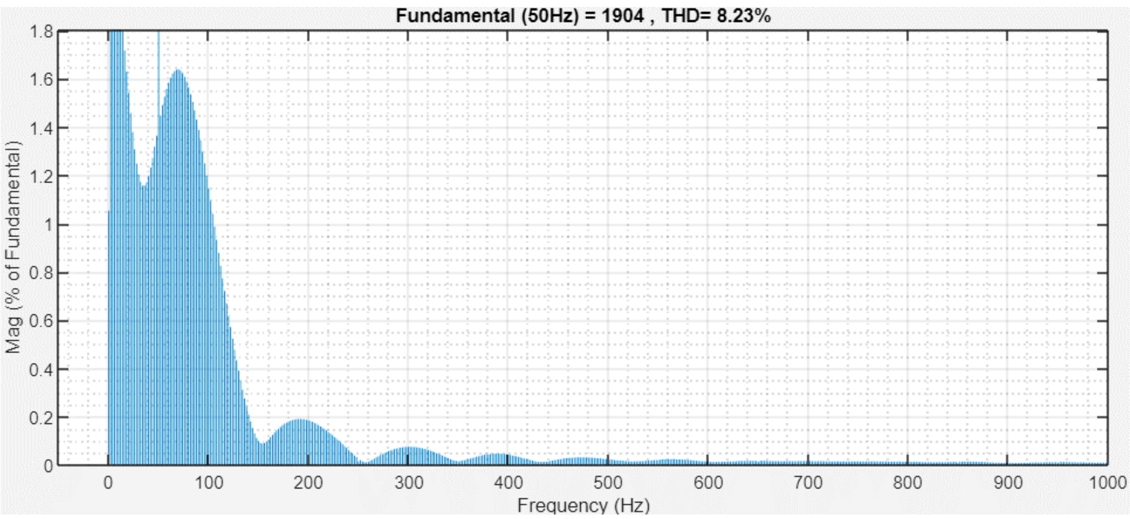

Figure 4. 18 THD for grid voltage with filter and without controller

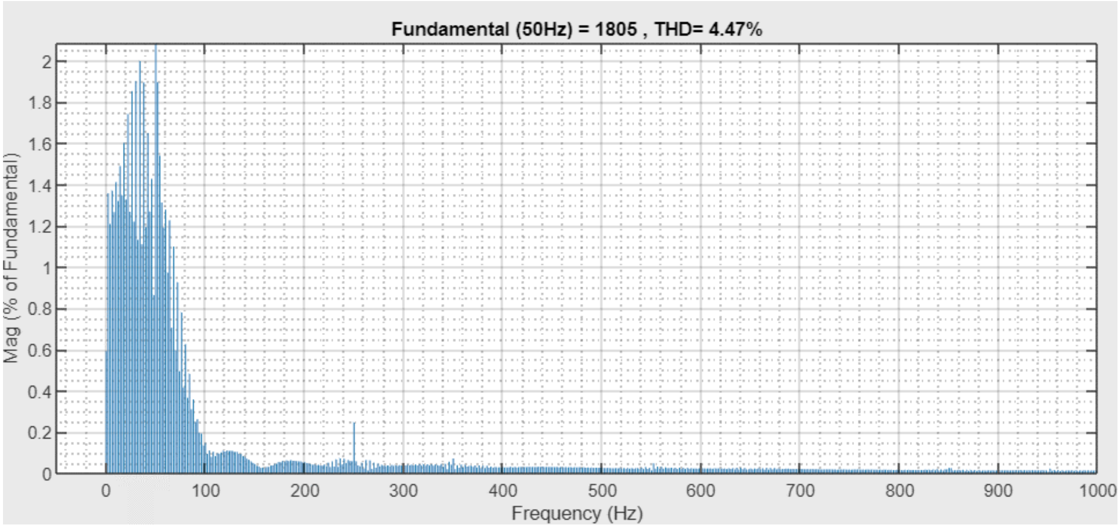

Figure 4. 19 THD for voltage with filter and controller

Figures 4.18 and 4.19 are the voltage harmonics with the same filter but with and without the controller. The primary purpose of the controller is to make a signal in the wind generation process. But in addition to stability, the controller removes some harmonics created during the generation of power for the grid. As seen from the figures above the amount of harmonics is reduced from 8.23% to 4.43%. the amount of decrement is almost 3.8% after the addition of the controller

CHAPTER FIVE

5. CONCLUSION AND RECOMMENDATION

5.1 Conclusion

In this thesis, investigate the impact of integrating wind power into the grid on power quality during dynamic operations. I compared two scenarios: one using an open loop with filter output and the other employing robust slide mode control, which addresses common issues in conventional sliding mode control methods.

By employing a unique smooth continuous function, the robust slide mode control enhances performance and stability, overcoming chattering challenges. I evaluate my methodologies based on criteria like voltage total harmonic distortion and active/reactive power, modeling essential components such as the PMSG and converters in MATLAB/Simulink.

Comparing the outcomes, robust slide mode control shows significant improvements, notably reducing total harmonic distortion to 4.43%, meeting IEEE 519 criteria. This simulation data and analysis confirm the effectiveness of our proposed control technique, especially in wind power systems using PMSG variable speed technology.

5.2 Recommendations for Future Work

The whole system in this thesis is designed and simulated only in Matlab/Simulink. In most work, simulation software may not show the exact operation of the wind energy system and testing of the controllers. Hardware is not designed in this system due to the high cost of the material and there is not enough access to material in our country. The author recommends future testing by designing simple hardware if materials are easy to access.

In this system, most control systems in MPPT and pitch angle together with MSC and GSC are designed in conventional PI controller form. This is due to a limitation of control system design knowledge. Therefore, it is better to add extra control techniques like artificial intelligence in MPPT for increasing power and other controllers in the grid for better performance.

REFERENCE

Abdelateef Mostafa, M., El-Hay, E. A., & ELkholy, M. M. (2023). Recent Trends in Wind Energy Conversion System with Grid Integration Based on Soft Computing Methods: Comprehensive Review, Comparisons and Insights. In *Archives of Computational Methods in Engineering* (Vol. 30, Issue 3). Springer Netherlands. https://doi.org/10.1007/s11831-022-09842-4

Ahmed, S. D., Al-Ismail, F. S. M., Shafiullah, M., Al-Sulaiman, F. A., & El-Amin, I. M. (2020). Grid Integration Challenges of Wind Energy: A Review. *IEEE Access*, *8*, 10857–10878. https://doi.org/10.1109/ACCESS.2020.2964896

Arachchige, L. N. W., Rajapakse, A. D., & Muthumuni, D. (2017). Implementation, comparison and application of an average simulation model of a wind turbine driven doubly fed induction generator. *Energies*, *10*(11). https://doi.org/10.3390/en10111726

Aroussi, H. A., Ziani, E., Bouderbala, M., & Bossoufi, B. (2020a). Improvement of direct torque control applied to doubly fed induction motor under variable speed. *International Journal of Power Electronics and Drive Systems*, *11*(1), 97–106. https://doi.org/10.11591/ijpeds.v11.i1.pp97-106

Aroussi, H. A., Ziani, E. M., Bouderbala, M., & Bossoufi, B. (2020b). Enhancement of the direct power control applied to DFIG-WECS. International Journal of Electrical and Computer Engineering, 10(1), 35–46. https://doi.org/10.11591/ijece.v10i1.pp35-46

Bekri, O. L., Fellah, M. K., & Benkhoris, M. F. (2014). Impact of the wind generator on the power flow in the electric grid. 3rd International Symposium on Environment Friendly Energies and Applications, EFEA 2014, February 2015. https://doi.org/10.1109/EFEA.2014.7059945

Beltran, B., Benbouzid, M. E. H., & Ahmed-Ali, T. (2012). Second-order sliding mode control of a doubly fed induction generator driven wind turbine. IEEE Transactions on Energy Conversion, 27(2), 261–269. https://doi.org/10.1109/TEC.2011.2181515

Benamor, A., Benchouia, M. T., Srairi, K., & Benbouzid, M. E. H. (2019). A new rooted tree optimization algorithm for indirect power control of wind turbine based on a doubly-fed induction generator. ISA Transactions, 88, 296–306. https://doi.org/10.1016/j.isatra.2018.11.023

Blaabjerg, F., & Ma, K. (2017). Wind Energy Systems. Proceedings of the IEEE, 105(11), 2116–2131. https://doi.org/10.1109/JPROC.2017.2695485

Blooming, T. M., & Carnovale, D. J. (2006). Application of IEEE std 519-1992. *Ieee*, 1–9. https://www.eaton.com/content/dam/eaton/products/backup-power-ups-surge-it-power-distribution/power-conditioners/harmonic-correction-unit/IEEE-std-519-1992-harmonic-limits.pdf

Bossoufi, B., Karim, M., Lagrioui, A., Taoussi, M., & Derouich, A. (2015). Observer backstepping control of DFIG-Generators for wind turbines variable-speed: FPGA-based implementation. *Renewable Energy*, *81*, 903–917. https://doi.org/10.1016/j.renene.2015.04.013

Bubshait, A. S., Mortezaei, A., Simoes, M. G., & Busarello, T. D. C. (2017). Power Quality Enhancement for a Grid Connected Wind Turbine Energy System. IEEE Transactions on Industry Applications, 53(3), 2495–2505. https://doi.org/10.1109/TIA.2017.2657482

Dash, R. L., Tripathy, S., Mohanty, B., & Hota, P. K. (2021). Power Quality Improvement of Grid Connected Wind System with STATCOM. ICPEE 2021 - 2021 1st International Conference on Power Electronics and Energy. https://doi.org/10.1109/ICPEE50452.2021.9358720

Echiheb, F., Ihedrane, Y., Bossoufi, B., Bouderbala, M., Motahhir, S., Masud, M., Aljahdali, S., & ElGhamrasni, M. (2022). Robust sliding-Backstepping mode control of a wind system based on the DFIG generator. Scientific Reports, 12(1), 1–16. https://doi.org/10.1038/s41598-022-15960-7

Elkodama, A., Ismaiel, A., Abdellatif, A., Shaaban, S., Yoshida, S., & Rushdi, M. A. (2023). Control Methods for Horizontal Axis Wind Turbines (HAWT): State-of-the-Art Review. Energies, 16(17). https://doi.org/10.3390/en16176394

Freire, N., Estima, J., & Cardoso, A. (2012). A comparative analysis of PMSG drives based on vector control and direct control techniques for wind turbine applications. Przeglad Elektrotechniczny, 88(1 A), 184–187.

Gharib-Yosry, A., Blanco-Marigorta, E., Fernández-Jiménez, A., Espina-Valdés, R., & Álvarez-álvarez, E. (2021). Wind–water experimental analysis of small sc-darrieus turbine: An approach for energy production in urban systems. Sustainability (Switzerland), 13(9). https://doi.org/10.3390/su13095256

González, L. G., Figueres, E., Garcerá, G., & Carranza, O. (2010). Maximum-power-point tracking with reduced mechanical stress applied to wind-energy-conversion-systems. Applied Energy, 87(7), 2304–2312. https://doi.org/10.1016/j.apenergy.2009.11.030

Grant, J., Manager, G., & Uk, C. A. (n.d.). Power Quality Issues - Part 4 - Voltage Imbalance. 3–5.

Guo, Z., Zhang, J., Sun, Z., & Zheng, C. (2017). Indirect Field Oriented Control of Three-phase Induction Motor Based on Current-source Inverter. Procedia Engineering, 174, 588–594. https://doi.org/10.1016/j.proeng.2017.01.192

Gustavo, M., & Enrique, P. (2011). Modelling and Control Design of Pitch-Controlled Variable Speed Wind Turbines. Wind Turbines, April 2011. https://doi.org/10.5772/15880

Hailu, A. D., & Kumsa, D. K. (2020). Ethiopia renewable energy potentials and current state. AIMS Energy, 9(1), 1–14. https://doi.org/10.3934/ENERGY.2021001

Hammoumi, D., El Bekkali, C., Karim, M., Taoussi, M., El Ouanjli, N., & Bossoufi, B. (2019). Direct controls for wind turbine with PMSG used on the real wind profile of essaouira-Morocco City. Indonesian Journal of Electrical Engineering and Computer Science, 16(3), 1229–1239. https://doi.org/10.11591/ijeecs.v16.i3.pp1229-1239

Hamzah, A., Suwitno, S., Irfan, J., Kurniawan, I., Gussyafri, H., Susanto, H., & Tsitsino, T. (2020). Design and Simulation of Permanent Magnet Synchronous Generators for Small Scale Wind Power Plants. E3S Web of Conferences, 190, 1–8. https://doi.org/10.1051/e3sconf/202019000001

Harish, V. S. K. V., & Sant, A. V. (2021). Grid integration of wind energy conversion systems. Handbook of Environmental Chemistry, 99, 45–66. https://doi.org/10.1007/698_2020_610

Jayathilake, R. (2017). Design of Wind Turbine Semester Project. July, 40. https://doi.org/10.13140/RG.2.2.11392.74243

Jin, N., Wang, X., & Wu, X. (2014). Current sliding mode control with a load sliding mode observer for permanent magnet synchronous machines. Journal of Power Electronics, 14(1), 105–114. https://doi.org/10.6113/JPE.2014.14.1.105

Johnson, G. L. (2001). Wind Energy System. 384.

Karaoui, I. El, Maaroufi, M., & Bossoufi, B. (2022). Fuzzy sliding mode power control for wind power generation systems connected to the grid. International Journal of Power Electronics and Drive Systems, 13(1), 606–619. https://doi.org/10.11591/ijpeds.v13.i1.pp606-619

Karim, M., Taoussi, M., Alami-aroussi, H., & Bouderbala, M. (2016). Rooted Tree Optimization for Backstepping Power Control of DFIG Wind Turbine : dSPACE Implementation.

Kasem Alaboudy, A. H., Daoud, A. A., Desouky, S. S., & Salem, A. A. (2013). Converter controls and flicker study of PMSG-based grid connected wind turbines. Ain Shams Engineering Journal, *4*(1), 75–91. https://doi.org/10.1016/j.asej.2012.06.002

Laghari, B. A., Soomro, M. A., & Shaikh, M. M. (2020). Power Quality Assessment of Small scale grid integrated DFIG based WECS Power Quality Assessment of Small scale grid integrated DFIG based WECS under balanced and unbalanced conditions. February. https://doi.org/10.2019/IJEDI.2582.0788/202001002

M. Saad, M. M. (2014). Comparison of Horizontal Axis Wind Turbines and Vertical Axis Wind Turbines. IOSR Journal of Engineering, 4(8), 27–30. https://doi.org/10.9790/3021-04822730

Madhu, R. K., & Mathew, A. (2013). Matlab/Simulink Model of Field Oriented Control of Pmsm Drive Using Space Vectors. International Journal of Advances in Engineering & Technology, 6(3), 1355–1364.

Mahammadsoaib, M. S., & Sajid, M. P. (2015). Notice of Removal: Vector controlled PMSM drive using SVPWM technique - A MATLAB / simulink implementation. International Conference on Electrical, Electronics, Signals, Communication and Optimization, EESCO 2015, February. https://doi.org/10.1109/EESCO.2015.7253938

Mahfoud, M. El, Bossoufi, B., Ouanjli, N. El, Said, M., & Taoussi, M. (2021). Improved Direct Torque Control of Doubly Fed Induction Motor Using Space Vector Modulation. International Journal of Intelligent Engineering and Systems, 14(3), 177–188. https://doi.org/10.22266/ijies2021.0630.16

Mahmoud, M. M., Hemeida, A. M., Senjy, T., & Ewais, A. M. (2019). Fault Ride-Through Capability Enhancement for Grid-Connected Permanent Magnet Synchronous Generator Driven by Wind Turbines. IEEE Conference on Power Electronics and Renewable Energy, CPERE 2019, 567–572. https://doi.org/10.1109/CPERE45374.2019.8980139

Maihemuti, S., Wang, W., Wang, H., Wu, J., & Zhang, X. (2021). Dynamic Security and Stability Region under Different Renewable Energy Permeability in IENGS System. IEEE Access, *9*, 19800–19817. https://doi.org/10.1109/ACCESS.2021.3049236

Majout, B., Abrahmi, D., Ihedrane, Y., Bakkali, C. El, Mohammed, K., & Bossoufi, B. (2021). Improvement of sliding mode power control applied to wind system based on doubly-fed induction generator. International Journal of Power Electronics and Drive Systems, 12(1), 441–452. https://doi.org/10.11591/ijpeds.v12.i1.pp441-452

Majout, B., Bossoufi, B., Bouderbala, M., Masud, M., Al-Amri, J. F., Taoussi, M., El Mahfoud, M., Motahhir, S., & Karim, M. (2022). Improvement of PMSG-Based Wind Energy Conversion System Using Developed Sliding Mode Control. Energies, 15(5), 1–17. https://doi.org/10.3390/en15051625

Manyonge, A. W., Ochieng, R. M., Onyango, F. N., & Shichikha, J. M. (2012). Mathematical modelling of wind turbine in a wind energy conversion system: Power coefficient analysis. Applied Mathematical Sciences, *6*(89–92), 4527–4536.

Meghni, B., Dib, D., & Azar, A. T. (2017). A second-order sliding mode and fuzzy logic control to optimal energy management in wind turbine with battery storage. Neural Computing and Applications, 28(6), 1417–1434. https://doi.org/10.1007/s00521-015-2161-z

Mohamed, S. A., Abd, M., & Sattar, E. (2019). Dynamic Performance and Effectiveness of Voltage Disturbances on the Improvement of Power Quality for Grid-Connected DFIG System Based Wind Turbines. *5*(17), 25–30.

Molla, E. M., & Kuo, C. C. (2020). Voltage Sag Enhancement of Grid Connected Hybrid PV-Wind Power System Using Battery and SMES Based Dynamic Voltage Restorer. IEEE Access, 8, 130003–130013. https://doi.org/10.1109/ACCESS.2020.3009420

Mousa, H. H. H., Youssef, A. R., & Mohamed, E. E. M. (2019). Model predictive speed control of five-phase permanent magnet synchronous generator-based wind generation system via wind-speed estimation. International Transactions on Electrical Energy Systems, 29(5), 1–16. https://doi.org/10.1002/2050-7038.2826

Mousa, H. H. H., Youssef, A. R., & Mohamed, E. E. M. (2020). Optimal power extraction control schemes for five-phase PMSG based wind generation systems. Engineering Science and Technology, an International Journal, 23(1), 144–155. https://doi.org/10.1016/j.jestch.2019.04.004

Rafiee, Z., Rafiee, M., & Aghamohammadi, M. R. (2020). The voltage dip and doubly fed induction generator with considering uncertainty conditions. Bulletin of Electrical Engineering and Informatics, 9(1), 30–38. https://doi.org/10.11591/eei.v9i1.1669

Rehman, S., Mahbub Alam, M., Alhems, L. M., & Mujahid Rafique, M. (2018). Horizontal AxisWind Turbine Blade Design Methodologies for Efficiency Enhancement A Review. Energies, 11(3). https://doi.org/10.3390/en11030506

Rhaili, S. E., Abbou, A., Marhraoui, S., Moutchou, R., & El Hichami, N. (2020). Robust sliding mode control with five sliding surfaces of five-phase PMSG based variable speed wind energy conversion system. International Journal of Intelligent Engineering and Systems, 13(4), 346–357. https://doi.org/10.22266/IJIES2020.0831.30

Senapati, S. K. (2014). Modelling and Simulation of a Grid Connected Doubly Fed Induction Generator for Wind Energy Conversion System. 2014.

Singh, B., Al-haddad, K., Member, S., & Chandra, A. (1999). Power Quality Improvement. October, 46(5), 960–971.

Sun, H., Qiu, C., Lu, L., Gao, X., Chen, J., & Yang, H. (2020). Wind turbine power modelling and optimization using artificial neural network with wind field experimental data. Applied Energy, 280(July), 115880. https://doi.org/10.1016/j.apenergy.2020.115880

Tang, L., Han, Y., Yang, P., Wang, C., & Zalhaf, A. S. (2022). A review of voltage sag control measures and equipment in power systems. *Energy* Reports, 8, 207–216. https://doi.org/10.1016/j.egyr.2022.05.158

Yin, X. xing, Lin, Y. gang, Li, W., Gu, Y. jing, Liu, H. wei, & Lei, P. fei. (2015). A novel fuzzy integral sliding mode current control strategy for maximizing wind power extraction and eliminating voltage harmonics. Energy, 85, 677–686. https://doi.org/10.1016/j.energy.2015.04.005

Yıldız, C., Keçecioğlu, Ö. F., Açıkgöz, H., Gani, A., & Şekkeli, M. (2015). Power Quality Measurement and Evaluation of a Wind Farm Connected to Distribution Grid. Procedia - Social and Behavioral Sciences, 195, 2370–2375. https://doi.org/10.1016/j.sbspro.2015.06.211

Zhang, Z., & Shu, J. (2010). Matlab-based permanent magnet synchronous motor vector control simulation. Proceedings - 2010 3rd IEEE International Conference on Computer Science and Information Technology, ICCSIT 2010, 9, 539–542. https://doi.org/10.1109/ICCSIT.2010.5563610

APPENDICES

Appendix A:MATLAB Script for Over All System

```
Rs=6.25e-3;                 % Stator resistance (ohm)
Ld=0.395e-3;                % Inductance of d-axis
Lq=0.395e-3;                % Inductance of q-axis
p=44;                       % Number of pole pair
flux=11.1464;
Lf=5e-4;                    % Inductance of filter
Rf=0;                       % Resistance of filter
Cbus=0.06;                  % DC bus capacitance
Vdcref=5000                 % DC bus reference voltage
Ts=10e-6;
eps=0.707;
R=77;                       % Length of the blade
rho=1.225;                  % Air density
J=10000;                    % Inertia
F=0;
%%wind turbine constants
cpmax=0.45;                 % Power coefficient
lamopt=6.14;                % optimum tip speed ratio
K=1;
c1=0.5176;
c2=116;
c3=0.4;
c4=5;
c5=21;
c6=0.0086;
%%turbine
wnvitesse=2*pi/0.09;
kpv=2*eps*wnvitesse*J;
kiv=wnvitesse*wnvitesse*J;
Widr=2*pi/40e-03;
Kid=Lf*((Widr)^2);
```

```
Kpd=(2*eps*Lf*Widr)-Rs;
Wiqr=2*pi/40e-03;
Kiq=Lf*((Wiqr)^2);
Kpq=(2*eps*Lf*Wiqr)-Rs;
% Grid side converter
Wudc=2*pi/200e-03;
Ki=Cbus*((Wudc)^2);
Kp=Cbus*2*eps*Wudc;
wpll=2*pi/0.07;
kpPLL=2*eps*wpll;
DiPLL=2*eps/(wpll);
kiPLL=kpPLL/DiPLL;
KiQr=0.2;
KpQr=0.017;
% Machine side converter
Kdn=500e60;
Kqn=50000e10;
```

Appendix B:MATLAB Simulink

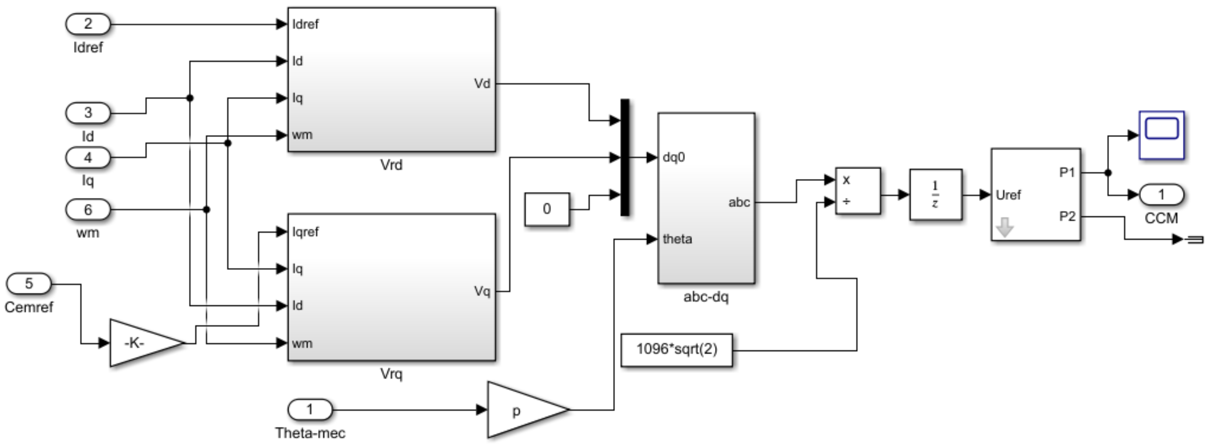

Figure B. 1 Simulink model of Machine side control

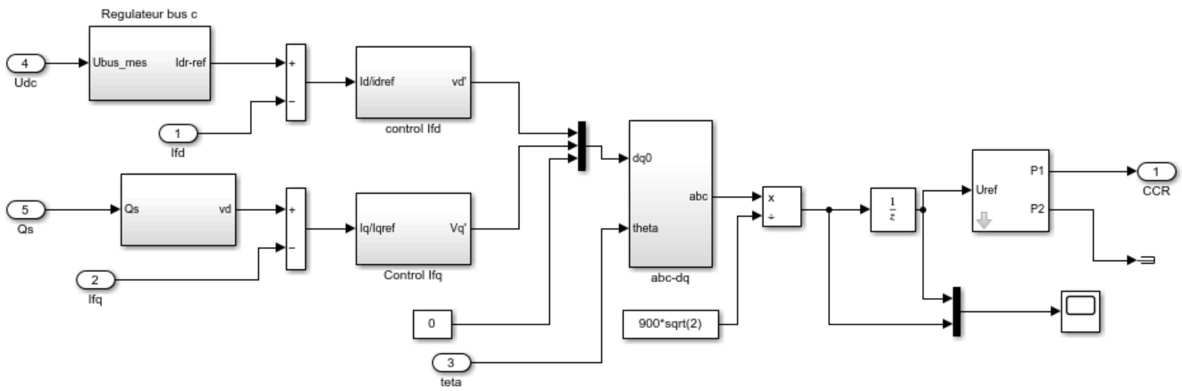

Figure B. 2 Simulink model of Grid Side control

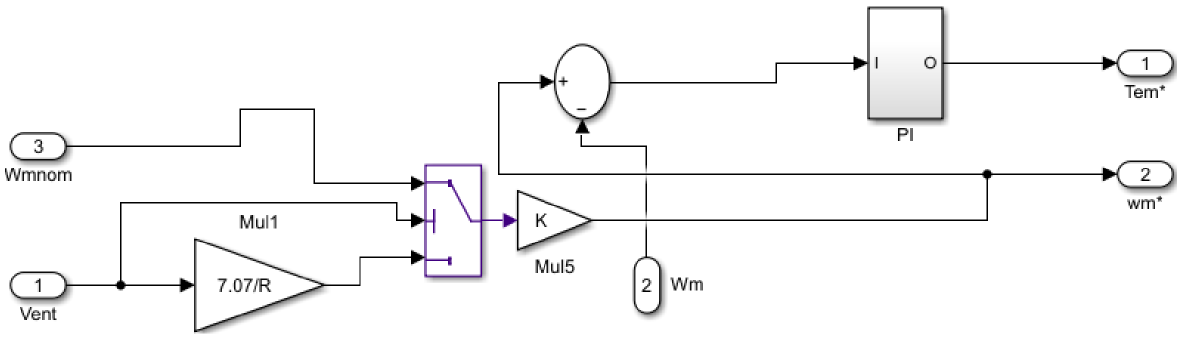

Figure B. 3 Simulink model of MPPT control

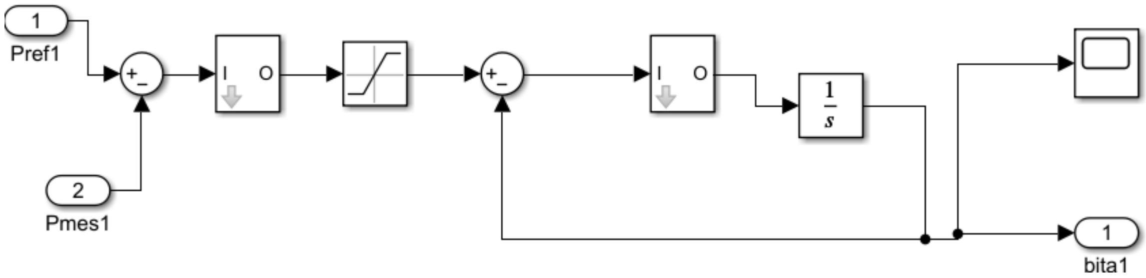

Figure B. 4 Simulink model of Pitch angle control

Appendix C: Adama I Wind Turbine Generator and Turbine data

Table C. 1 Adama I Wind Turbine Generator and Turbine data

Parameter	Value
Wind turbine nominal power	1.5 MW
No wind turbine	34
Wind turbine inertia constant(H/s)	4.32
Rotor diameter	77 m

Wind turbine rotor radius	37.3 m
Cut in speed	3 m/s
Cut out speed	22 m/s
Rated speed	11 m/s
Optimal speed ratio	6.14
Maximum power coefficient	0.45
No of blade	3
Rated mechanical power	1.5 MW
Rated apparent power	1.6 MVA
Generator inertia	3500 J/kg.m2
Rated power factor	0.97
Rated speed	17.3 rpm
No pole pair	44
Rated rotor flux linkage	1.48
Stator winding resistance	0.006
d-axis synchronous inductance	0.395 mH
Q-axis synchronous inductance	0.395 mH
Rated current	680 A

Appendix D: PI Control Parameter

Table D. 1 PI Control Parameter

Parameters	Gain value	
	Kp	Ki
Dc bus voltage	2.6653	59.2176
Current controller d-axis	0.1048	12.3374
Current controller q-axis	0.1048	12.3374
Pll controller	126.9203	8.0568
Reactive power controller	0.017	0.2